NASA Contractor Report 185225

Advanced Instrumentation for Aircraft Icing Research

W. Bachalo, J. Smith, and
R. Rudoff

Aerometrics, Inc.
Sunnyvale, California

April 1990

Prepared for
Lewis Research Center
Under Contract NAS3-25317

National Aeronautics and
Space Administration

TABLE OF CONTENTS

1.0 INTRODUCTION

Aircraft icing research remains as a vital activity in the advancement of commercial and general aviation safety as well as to military airborne operations[1,2,3,4]. Ice accretion occurs when an aircraft encounters a cloud of supercooled liquid drops. Because of the large relative velocities between the aircraft and the drops, impaction and freezing of the drops on the aircraft components takes place. Latent heat of fusion is convected away by the surrounding air flow. Formation of the ice on the airfoil in the classic horn shape serves to dramatically increase the drag and may affect the control surfaces due to flow separation. The increase in fuel consumption and loss of control often leads to disaster. It is said that inexperienced general aviation pilots only encounter icing conditions once in their lives.

Helicopter icing is an even more serious problem since these aircraft frequently need to operate at altitudes subject to icing conditions and their missions generally do not allow avoidance by flying around icing clouds as do commercial fixed wing aircraft [5,6,7,8,9]. Currently, there is an increasing need for helicopters to be able to operate in forecasted icing conditions for both military and civilian operations. The rotor icing presents one of the most complex problems to icing research. Ice build up and release not only affects the performance but also may seriously compromise the stability and control of the

aircraft. The flow field is highly three-dimensional and unsteady so it is not easy to compute the drop trajectories and hence, the ice accretion. Thus, careful experimentation is required that must cover a wide range of parametric conditions.

De-icing the aircraft engine nacelles, wing leading edges, and other components require improvements in design and performance. Although current systems are effective, their reliability and efficiency requires improvements. This is especially true in the case of helicopters. Very few civilian helicopters are icing certified by the FAA. Because of the range of rotor flow and loading conditions due to changes in collective, Mach number, rotational speed, blade geometry, flexibility, and other conditions the problem of icing protection is significantly more complex than for fixed wing aircraft. It is evident that the computational efforts will need a great deal of support from good detailed experiments in both ground-based and flight facilities.

In order to improve upon the science of ice accretion and icing protection systems, several requirements need to be satisfied. First of all, a sound data base on the nature of icing clouds is necessary. Wind tunnels and flight facilities must be available that can provide reliable simulations of the icing cloud conditions including temperatures and cloud drop size distributions. Finally, reliable instrumentation must be available to verify the conditions, especially the drop size distributions and

liquid water content (LWC). Of these requirements, there is a general lack of confidence in the cloud drop size distribution and LWC data, in the ability to simulate these clouds, and in the instrumentation used to characterize the simulated clouds. Elimination of the problems with the instrumentation is the objective of this proposed research.

In situ cloud drop size measurements have been accomplished using slide impaction techniques and optics-based probes[10,11,12,13,14]. In general, the slide impaction methods are considered reliable but very tedious and hence, good statistical representations of the size distributions are not always obtained. In most work over the past decade or more, the well-known light scatter detection and shadowing probes developed by PMS, Inc of Boulder, Colorado have been used extensively for atmospheric or meteorology studies and in the wind tunnels. The details of these probes are presented in many publications as are reports on their performance.

The PMS Forward Scattering Spectrometer (FSSP) and the Optical Array Probes (OAP) instruments purportedly measure the size distributions, number density, and liquid water content. A great deal of data have been obtained with these instruments. However, some studies have indicated that these data are not always reliable. There appears to be a lack of consistency in the results. That is, in some cases the data agrees with other measurements but in others the comparisons show quite large differences. This inconsistency also has

been observed between probes of the same type. Because of the limited size range of the FSSP, it often needs to be used with the OAP to complete the size distribution. Unfortunately, combining the size distributions does not always lead to satisfactory results in that the particle counts from the individual instruments do not agree in the overlap region of the distributions.

With the development of the Phase Doppler Particle Analyzer[15,16], the science of drop size characterization has been advanced considerably. This instrument performs measurements based upon the light wave length rather than the scattered intensity. The wave length is unaffected be the presence of optical components and drops in the optical path whereas the intensity is reduced. Furthermore, the PDPA requires only a single factory calibration whereas the light scatter intensity detection methods require relatively frequent calibration checks. The PDPA can cover a very wide range of particle sizes with simple changes in the detector gains and the optics and it has a dynamic size range of over a factor of 35 which is significantly greater than the PMS systems. Because simultaneous measurements of the drop velocity is obtained, the information on the drop dynamics is available including the angle of trajectory and velocity magnitude for each drop size class. With the in situ measurement of the size of the sampling volume the particle number density and liquid water content (LWC) can be obtained with good accuracy.

The significant advantages and capabilities of the phase Doppler method have been recognized world wide and the method is now accepted as the standard in drop size characterization. In this proposal, the development of a compact rugged probe based on the phase Doppler method for both icing research tunnel and airborne applications is described. A review of the feasibility study will provide information for the evaluation of the potential of this instrument and its advantages in fulfilling the measurement requirements in aircraft icing research. Design considerations will be reviewed with respect to the measurement environment and working conditions of the probe; namely the cold high vibration conditions of the windtunnel and aircraft and the requirement that the probe remain operational with little or no adjustment by the user. Finally, the steps of the development program will be outlined which will ensure that all aspects of the probe design and performance are thoroughly tested before the prototype is delivered for final testing at the NASA Lewis Research Center.

2.0 RESULTS OF PHASE I WORK

This section describes the work conducted in the Phase I research program. The Phase I program had the goal of providing the following general results with emphasis particularly devoted to the final result of building a probe for airborne and large scale wind tunnel applications:

1. Determination of the feasibility of applying the Phase Doppler Particle Analyzer (PDPA) to the in situ characterization of droplet field size distributions and liquid water content (LWC) for fog and clouds. The PDPA results were to be compared to results derived from other physical means.
2. LWC measurements obtained from the PDPA in a small scale spray chamber were to be compared to actual flow rates to evaluate the use of the PDPA for simultaneous LWC measurements.
3. Methodologies for discriminating liquid droplets from frozen drops and ice crystals will be examined.
4. Fiber optics technology will be evaluated as a means of building a compact, robust, and reliable probe for use in large scale icing research tunnels such as the NASA Lewis IRT and for use mounted on aircraft.

In order to meet these goals, the following research was conducted during the Phase I portion of this study. By

meeting these goals a good developmental baseline would be set to guide the development of an accurate and reliable probe in later phases of the research.

First, the PDPA methodology was thoroughly explored to determine its applicability to LWC measurements. Size distributions, number density, mass flux, and LWC were fully evaluated in a variety of conditions including sprays and simulated clouds in a wind tunnel. The standard PDPA was used for this evaluation. These data serve to validate the PDPA methodology in a cloud-type environment. Ice crystal rejection was also evaluated with the standard probe.

Next, development of a prototype fiber optic PDPA probe was undertaken. The previously verified PDPA method was transferred to a compact, waterproof and rugged probe. This prototype was primarily intended as a proof of concept for the fiber optic methodology. Hence, only minor considerations were made to airworthiness at this point. A number of decisions and evaluations of hardware had to be made during this design and development phase and they are reviewed in the following sections.

Testing of the probe was then initiated. The fiber optic probe was first compared to the standard probe in terms of accuracy and performance. Theses tests were performed in a small scale spray chamber.

The standard probe was also tested in a practical simulated spray at AEDC in an instrument comparison test. This was valuable in establishing performance in more

realistic environments. The PDPA was also compared to existing spray sizing instruments.

Finally, the opportunity arose to test the fiber optic probe in the IRT facility. The prototype probe was tested in the simulated cloud environment of the IRT at realistic temperatures. This testing revealed areas of the design requiring improvement and refinement prior to the fabrication of a final version of the fiber optic PDPA probe.

2.1 Phase Doppler Method

The basic PDPA instrument was developed under NASA Lewis and AFOSR funding to determine particle size and velocity distributions simultaneously in a spray. The theory was developed by Bachalo[17] and the instrument described by Bachalo and Houser.[15]

2.1.1 Theoretical Description

The need to measure particles to sizes larger than approximately 50 um in diameter, with good resolution, suggested the analysis of light scattered by reflection or refraction rather than by diffraction. The light scattered by diffraction is relatively independent of the index of refraction. The angular distribution of the forward scattered light is given by

$$S_{diff}(\alpha,\theta) = \alpha^2 \left[\frac{J_1(\alpha \sin\theta)}{\alpha\theta}\right] \qquad (.1)$$

where,

$$\alpha = \frac{\pi d}{\lambda} \qquad (.2)$$

is the scattering angle, J_1 is the first order Bessels function of the first kind, d is the diameter of the particle, and λ is the wavelength of the incident light. For large drops, the scattered intensity becomes concentrated along the transmitted beam and is, thus, very sensitive to angular resolution.

The angular distribution of light scattered by reflection and refraction is independent of drop-size except for the higher frequency resonant lobes produced by interference between the scattering components. The measurement of energy scattered at angles away from the forward direction (greater than 20^0) can be used to avoid the light scattered by diffraction. A detailed treatise of the scattering phenomena is given by van de Hulst.[18]

Bachalo[17], derived a theory for drop sizing using the phase shift of light transmitted through or reflected from spherical particles. Based on the analysis given by van de Hulst, the optical path length of a light ray passing through a sphere relative to a reference ray deflected at the center of the sphere is given by,

$$\phi_R = 2\alpha(sin\tau - pm\,sin\tau') \qquad (.3)$$

where p is a parameter that characterizes the emerging rays and relates to the interface from which it emerges. For

example, p = 0 for the first surface reflection, p = 1 for the transmitted ray, and p = 2 for the ray emerging after one internal reflection, m is the index of refraction, and ' are the angles between the surface tangent and the incident and refracted rays, respectively.

The phase shift with respect to the reference ray given by Eq.(3) can be inferred from light scattering interferometry produced with a standard dual beam laser Doppler velocimeter because the rays from each beam are incident upon the drop at different optical paths. Neglecting the phase shifts at reflection and focal lines, the relative phase shift due to the differing optical paths is described as,

$$\phi = \frac{2\pi d}{\lambda}\{(sin\tau_1 - sin\tau_2) - pm(sin\tau_1' - sin\tau_2')\} \qquad (.4)$$

where the subscripts represent beams 1 and 2. Since the angles are fixed by the receiver geometry, the phase only changes as a result of drop diameter d. The phase difference produces an interference fringe pattern which can be analyzed to obtain the drop size and velocity of the spherical particle. The temporal frequency of the fringe pattern is the Doppler difference frequency which is a function of the beam intersection angle, laser wavelength, and the velocity of the drop. The spatial frequency of the fringe pattern is dependent upon the beam intersection angle, laser wavelength, drop diameter, angle of observation, and drop index of refraction.

A direct means of measuring the interference pattern was developed by Bachalo and Houser.[15] The scheme uses pairs of detectors located at known angles to the laser beam and separated by fixed spacings, figures 2.1 and 2.2. As the drop passes through the beam intersection region, it produces a scattered interference pattern which appears to move past the receiver. Doppler burst signals with a relative phase shift are produced by each of the detectors. The phase shift is linearly related to the drop size. Changing the optical parameters which include laser beam intersection angle, collection angle, drop index of refraction, laser wavelength, and scattering component detected can be used to change the measurement of a drop size range.

Three detectors are required to extend the measurement range while maintaining good sensitivity. The two phase angles also serve as redundant measurements for additional testing of the signals and extend the size range sensitivity at one optical setting to a factor of approximately 100. Because drops scatter light in proportion to their diameter squared, the required detector response is 10^3 for a size range of 35, which limits the practical dynamic range of the instrument.

The PDPA on-line signal processing and data management computer stores a data packet for each drop measured which includes the drop size, velocity, and time of arrival. These measurements of are processed, transferred and stored

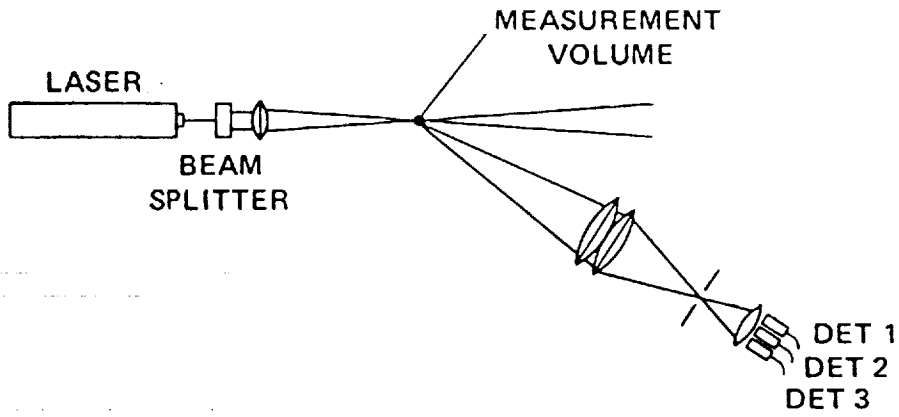

Figure 2.1 Schematic of the Phase Doppler Particle Particle Analyzer

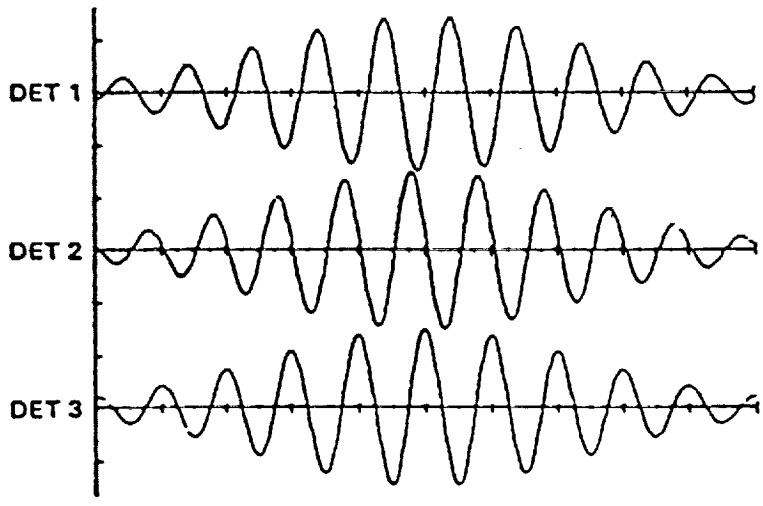

Figure 2.2 High Pass Filtered Doppler Bursts Illustrating the Phase Shift

in computer memory at a rate greater than 100,000 samples per second. Data is stored by direct memory access (DMA) and processed at the same time at a continuous rate of approximately 1000 samples per second. Thus, the size and velocity distributions are plotted on the monitor in essentially real time.

Such high data rates are required to ensure that the drop arrivals which are Poisson distributed are not missed when they pass through the sample volume at close intervals. For accurate number density measurements, it is important that the processing rate is sufficient to handle the smallest inter-particle arrival times. Average data rates as high as 5000-15,000 samples per second have been experienced in actual spray measurements. The highest arrival rate or inter-drop arrival time can vary by an order of magnitude from the average.

Assuming that the airflow and spray are thermodynamically in steady state (or by using conditional sampling in unsteady flows), the time averages are used to obtain the mean and rms fluctuating velocities for each size class. That is, all of the measurements of drop size, velocity, and time of arrival are stored in memory. The data can be processed to form a velocity probability density function for each size class. A mean and rms velocity for each size class can then obtained using,

$$\bar{U}(d_i) = \sum_{j=1}^{N} \frac{U(d_i,t)}{N} \qquad (.5)$$

and

$$\langle U'(d_i)\rangle = \sqrt{\frac{1}{N}\sum_{i=1}^{N}\left(U_i(d_i,t) - \bar{U}(d_i)\right)^2} \qquad (.6)$$

where the summation is taken over all the 50 drop size classes. $U_i(d,t)$ are the velocities of individual drops of size class d. Typically, 10,000 or more instantaneous drop measurements are acquired at each point in the flow field.

The measurements of the transverse velocity component and in regions with recirculation usually require frequency shifting. Frequency shifting causes the interference fringe patterns to appear to move at the shift frequency. This frequency offset allows the measurement of small transverse velocity components and the resolution of the directional ambiguity in recirculating flows. Frequency shifting also serves to compress the Doppler frequency bandwidth which allows the processing of an increased turbulence frequency bandwidth.

The individual drop size measurements are accumulated in histogram form to obtain the size distribution and the various mean diameters. The mean diameters used in spray analysis, namely, arithmetic, surface, volume, and Sauter mean diameters, are obtained from the following expression:

$$\bar{D}_{pq} = \left(\frac{\sum_{i=1}^{N} d_i^p}{\sum_{i=1}^{N} d_i^q}\right)^{\frac{1}{p-q}}$$

where p, q are the subscripts which characterize an average mean diameter. For example, D_{10} is the arithmetic mean and D_{32} is the Sauter mean diameter, (SMD).

2.1.2 Signal Processing

LDV or PDPA signals which are characterized as "burst" signals consist of a pedestal component which is a result of the Gaussian intensity distribution of the laser beam and a Doppler or high-frequency component which arise from the motion of the interference fringes produced by the moving particle. Noise produced by distortions to the laser beams, flare light from reflection, or other sources of optical noise can deteriorate the signal.

The pedestal or low frequency component of the signal must be removed by a high-pass filter. The high pass filter cut-off must be set low enough to avoid excessive attenuation of the Doppler frequency information. The use of frequency shift, as earlier mentioned, can compress the frequency bandwidth that must be filtered. In addition low pass filtering is applied to remove the high frequency noise which is always present in a Doppler signal.

Several methods are available for processing LDV signals. The Aerometrics PDPA uses a counter processor which operates in the time domain. After the high-pass filtering to remove the pedestal, the signal is log amplified to compress the 10^3 intensity range of the scattered light to a more easily handled range. The zero crossings of the signal represent the period of the Doppler difference frequency, figure 2.3. The counter averages the period over the entire burst that rises above a three-level threshold. The threshold is set to allow detection of the

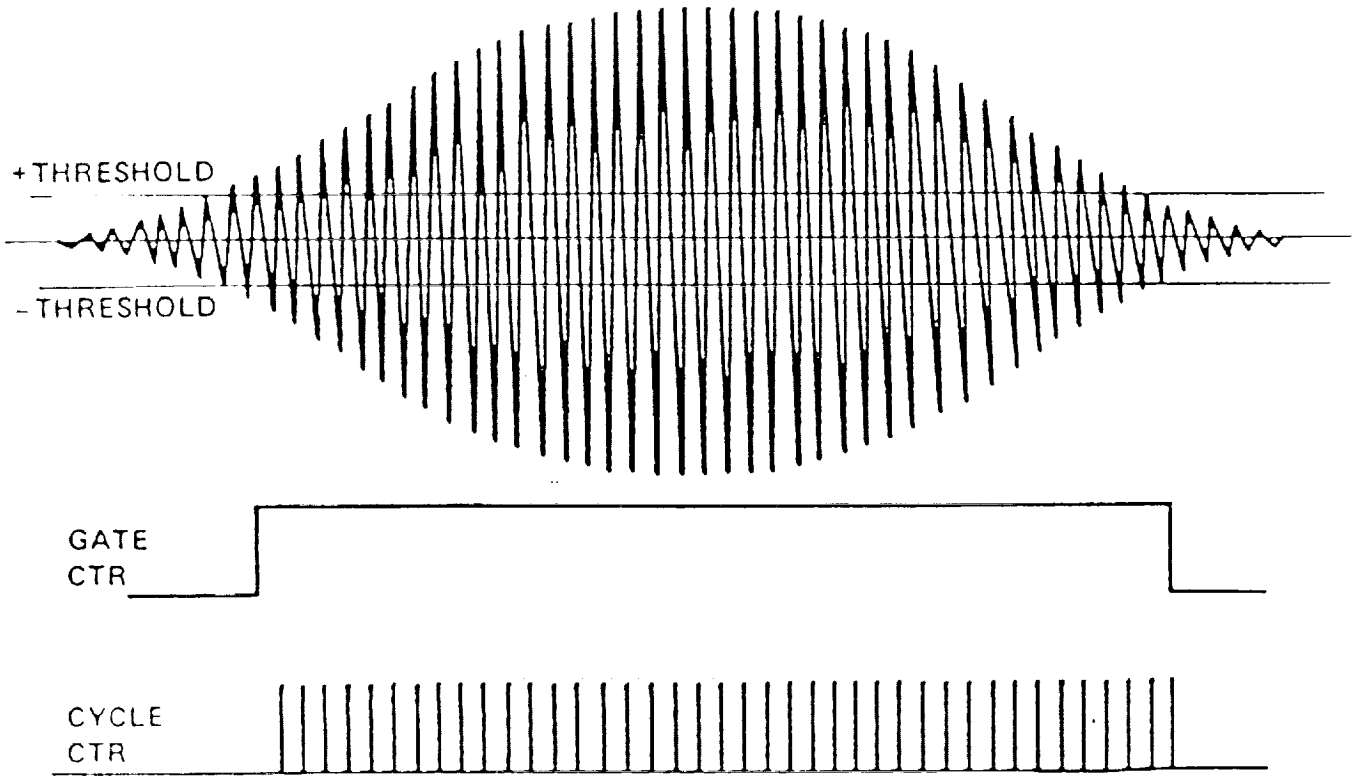

Figure 2.3 Counting Processor Principles

smallest particle size above the baseline noise. The log amplifier, allied with correct selection of PMT gain ensures that over the 35:1 dynamic range of the PDPA, both the smallest signals can be discerned, yet the largest particles signals do not saturate.

When the signal exceeds threshold, three counters are started. Two measure the Doppler period, while the other counts the number of cycles. Three sets of these counters are used to make the phase determination necessary for the PDPA size measurement.

2.1.3 PDPA Software

The Aerometrics PDPA software has been designed to allow rapid and intuitive keyboard access to the hardware parameters which may change during measurement. Changes in instrument setup, including frequency shift magnitude, PMT gain, filter setting and beam spacing (intersection angle) are performed directly from the keyboard. Automated routines to set PMT gain are incorporated in the software to help ensure reliable detection of all particles in the selected range and hence, accurate number density, flux and LWC calculations.

Quasi-real time graphic display of size and velocity distributions are updated as data is acquired. If alterations in the instrument setup are required, they can be performed rapidly from the computer keyboard.

Immediately after data collection at one location is completed, data analysis routines are available to display

the size-velocity correlation, volume distribution and other quantities of interest. Data is stored by a single command for later analysis if desired. Series of runs under different conditions may be stored as a unit and plots describing their behavior generated.

Overall, the PDPA software provides a powerful and rapid tool for making good quality drop size and velocity measurements. The simplicity of its operation allow the new user to initiate data acquisition in minimal time. The ease of altering instrument parameters during operation is essential in making measurements in rapidly changing, non-reproducible environments such as those encountered in clouds.

2.1.4 Evaluation of the PDPA Method

From a standpoint of measuring drop size and velocity accurately, the PDPA has been thoroughly evaluated in the past by many users. Sizing accuracy, both in comparison to other instruments, and from an absolute standpoint has been proven accurate.[16,19,20,21,22] More difficult is the accurate measurement of number density, volume flux and liquid water content (LWC) since all these quantities are interrelated and profoundly affected by the sample volume size. The effective sample volume size is different for each particle size due to the Gaussian nature of the laser beams. In addition to the data presented in this report, independent evaluation of number density and mass flux have been reported by Dodge.[23]

Sample Volume Size

Accurate measurement of the sampling cross-section for optical probes using Gaussian beam intensity distributions has been one of the more difficult tasks that need to be resolved to achieve accurate measurement of volume flux, number density and LWC. Early attempts used theoretical descriptions for focusing Gaussian beams to estimate sample volume cross-section. However the sampling volume cross-section for each particle size class depends, among other things, on the beam intensity, detector gains, threshold setting, and the quality of the Gaussian beams. A more promising approach was developed[15,25] and incorporated in the Aerometrics PDPA.

It was recognized that the interference fringes formed by the intersecting laser beams formed an intrinsic scale for the measurement of sample volume, figure 2.4. Particles have an equal possibility of passing on all trajectories through the sample volume. However, the greatest number of particles will have a higher probability of passing through the probe volume with a maximum number of fringe crossings, $N_{max}(d)$, followed by a lower likelihood of those particles with a trajectories crossing $(N_{max}(d) - 1)$ fringes, and so on. The maximum number of fringes, $N_{max}(d)$, for particles of diameter d, provides the desired beam diameter given by,

$$D_b = N_{max}(d)\,\delta$$

where the fringe spacing δ is given by,

$$\delta = \frac{\lambda}{2\sin(\gamma/2)}$$

and γ is the beam intersection angle. Since there is a minimum number of fringe crossings required for signal processing validation, the width, w(d), of the measurement cross-section is,

$$w(d) = \delta \left(N^2_{max}(d) - N^2_{min}(d) \right)^{1/2}$$

The length of the sampling cross-section along the beam axis is delineated by the width of the slit aperture in the receiver. Accurate determination of this length depends on the resolution of the receiver optics. An f/5 receiver is used with lenses designed for nominal 15 um resolution. With a slit aperture 100 um in width, this represents an uncertainty of 15%. Since the detectable diameter of the blur circle will be largest for the largest particles, this uncertainty will have the strongest influence on volume sensitive quantities such as D_{30} and volume flux. Particle number density is not as seriously affected because the smallest particles, which generally have the largest population, produce a much smaller detectable blur circle.

Figure 2.4 shows the fringe pattern which is used to generate the particle pathlengths through the beam. The measured cross-section is then used in the calculations of number density, volume flux and LWC. A sample curve

representing sample volume cross-section versus particle size is shown in figure 2.5. Experimental results are shown to agree well with a theoretical prediction. The procedure works well since it does not require, a priori, knowledge of the optical parameters determining beam waist diameter except for the intersection angle and laser wavelength, and accounts for all variations in the beam due to the measuring environment.

Number Density

In order to calculate LWC or the related quantity of volume flux, number density must be accurately determined. The number density is the number of particles per unit volume. In determining this quantity, the instrument counts the total number of particles, N_p, passing through the sample volume, A, during time interval, t. During this time the volume sampled is,

$$V = A\,t \sum_{i=1}^{50} n_i(d)\, u_i(d)$$

where $n_i(d)$ is the number of drops in drop size class i,and $u_i(d)$ is the mean velocity of each size class. Thus, the particle number density is $C_n = N_p/V$. Evaluations of the particle number density can be obtained by using beam extinction measurements and Beer's law. This method of evaluation is fully discussed by Bachalo.[24]

For the particle number density measurements, it is required that the swept volume of fluid be measured and the number of particles within the swept volume be accounted

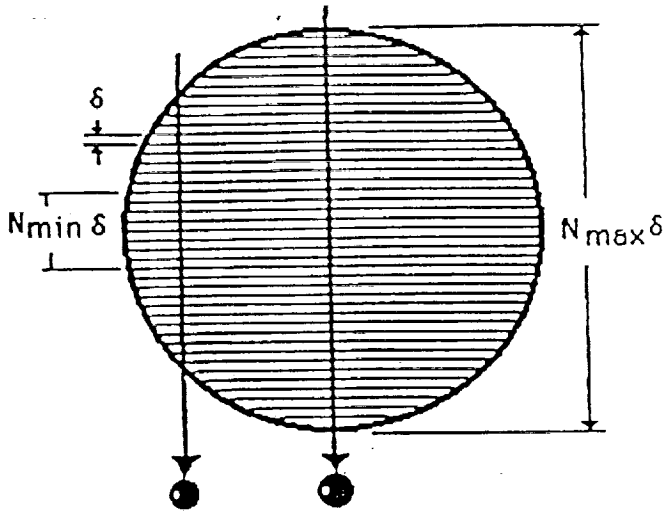

Figure 2.4 Schematic of the Sample Volume Showing the Implicit Fringe Pattern

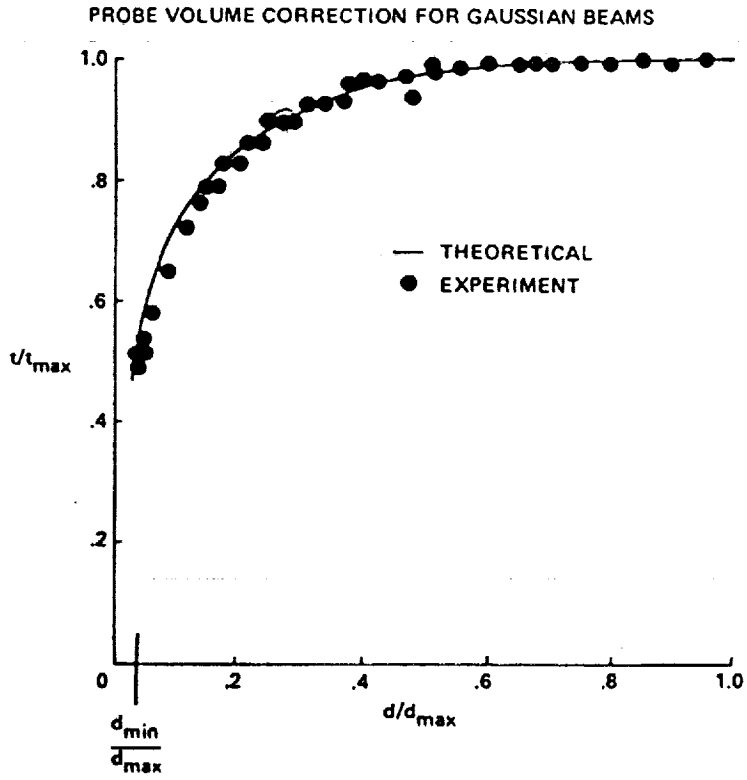

Figure 2.5 Variation of Sampling Cross Section with Particle Size

for. However, the swept volume for each size class must be used. This can become complicated by the fact that in some regions of the droplet field, drops in the same size class may be moving in a wide range of directions. In such cases, the swept volume computed from the average velocity could be erroneous leading to the conclusion that the number density is much greater than its actual value. It is the average spacing between particles passing through the sampling cross-section that is required. Thus, the absolute value (or magnitude) of the velocity is used in the measurement of particle number density for each size class. These values are then summed over all size classes.

Volume Flux and Liquid Water Content

The volume flux is calculated from the volume median diameter, D_{30}, the number of drops measured, N, and the sample volume cross-sectional area, A. It is given by,

$$F = \frac{\pi}{6} D_{30}^{3} \frac{N}{At} \qquad N = \sum_{i=1}^{50} N(\sigma_i)$$

A similar calculation for LWC may be made using D_{30} and the particle field number density, C_n, where now mean flow velocity is considered to derive a total volume in which the particles are found. Obviously, both of these measurements are interrelated. If one can be made accurately, so can the other value. Hence, data will be presented determining either quantity to validate the PDPA method. It is important to keep in mind the importance of an accurate sample volume cross-section determination if correct values

of volume mean diameter and number density are to be obtained.

Volume flux comparisons were made by measuring flux with the PDPA at one point in the spray and comparing it to the flux determined by a sharp edged orifice sampling probe located directly below the sample volume. The orifice had a cross-sectional area of 0.24 cm^2. LWC comparisons were made in a wind tunnel where spray nozzles produced a known droplet LWC throughout the test section.

Shown in figure 2.6 are measurements of number density and volume flux as a function of radial position within the spray cone of a simple pressure atomizer operated at 415 kPa. Excellent agreement is seen in the volume flux plot between the PDPA and the sampling probe. Excellent agreement has also been seen in high density sprays created by four impinging nozzles.[26]

An example of a number density evaluation with the PDPA is shown in figure 2.7. Number density and volume flux are plotted versus radial position for a liquid nitrogen spray. The 45^o, solid cone, pressure atomizer was operated at 690 kPa. Measurements were taken at three axial positions, x = 5, 10 and 16 cm below the atomizer. The table accompanying the plots compares the PDPA derived and extinction based transmittances which are dependent upon number density.

Excellent agreement was seen at the first two locations, while the extinction system was affected by the formation of ice crystals in the ambient air surrounding the

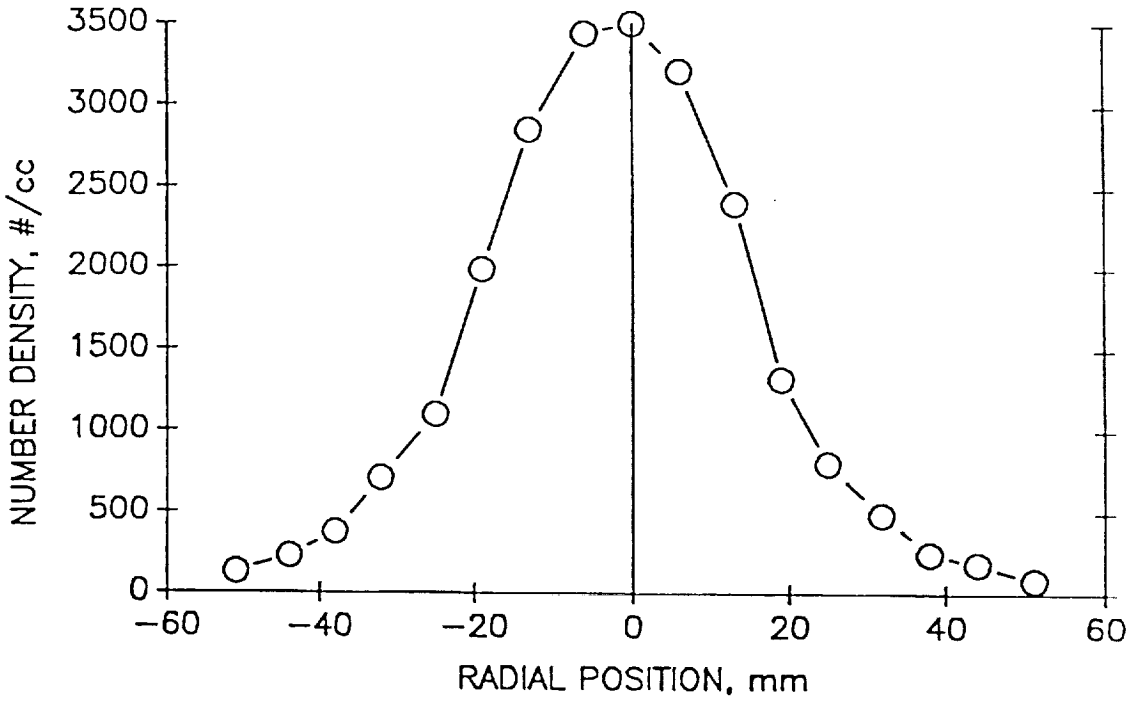

Figure 2.6 Radial Distribution of a) Number Density and b) Volume Flux for a Pressure Atomizer Operating at 415 kPa and Spraying Water

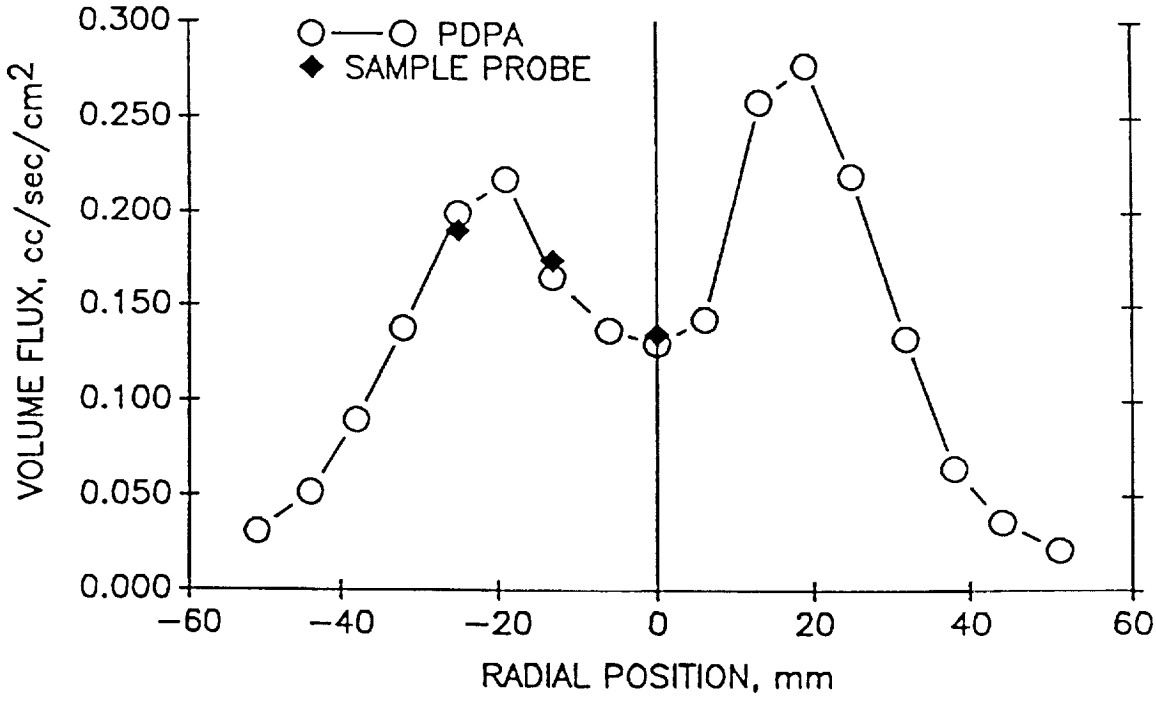

(cm) Axial Position	Transmittance (%) Extinction System	PDPA	Percent Difference
5	0.82	0.83	1.2
10	0.90	0.90	0.0
16	0.76	0.95	-20.0

Figure 2.7 Radial Distribution of a) Number Density and b) Volume Flux for a Pressure Atomizer Operating at 690 kPa and Spraying Liquid Nitrogen

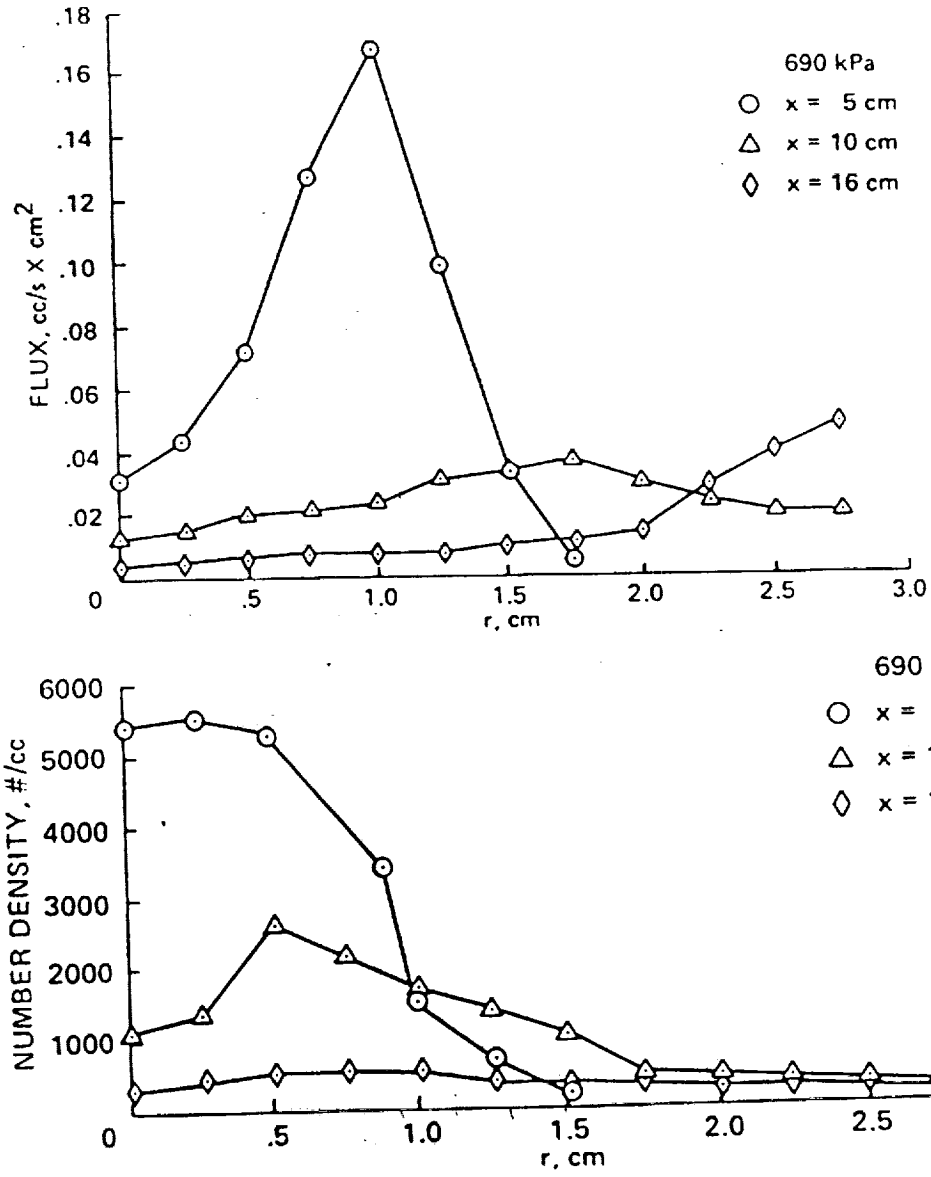

spray at x = 16 cm. The PDPA showed the expected further evaporation, possibly showing the instruments ability to reject ice crystals.

In the case of liquid nitrogen no direct sampling was attempted for volume flux. However, it is worthwhile to note the appreciable evaporation seen in the volume flux plot for the liquid nitrogen with increased axial distance.

Icing Tunnel Tests

A major test of PDPA performance in a simulated cloud environment was performed in a small scale icing tunnel. The tunnel was cooled to -18^{o} C with a free stream velocity of 67 m/s. The tunnel test section was approximately 38 cm square. A spray bar with multiple air-assist nozzles was located upstream of the contraction. The purpose of this spray bar was to produce a uniform LWC throughout the test section, but as will be seen when the data is examined this was not entirely the case.

Tests were performed at two water flow rates corresponding to values of LWC equal to 1.0 and 1.5 g/m^3. Nozzle air pressure was varied to alter the spray size distribution as depicted in the figure 2.8 plot of D_{30} versus atomizing air pressure. For low air pressures, the volume mean diameter, D_{30}, reached upwards of 45 um with many large drops as shown by the size and volume distributions in figure 2.9a. Note the large volume contribution of the few large particles. As the atomizing air to water flow ratio was increased, the D_{30} asymptoted

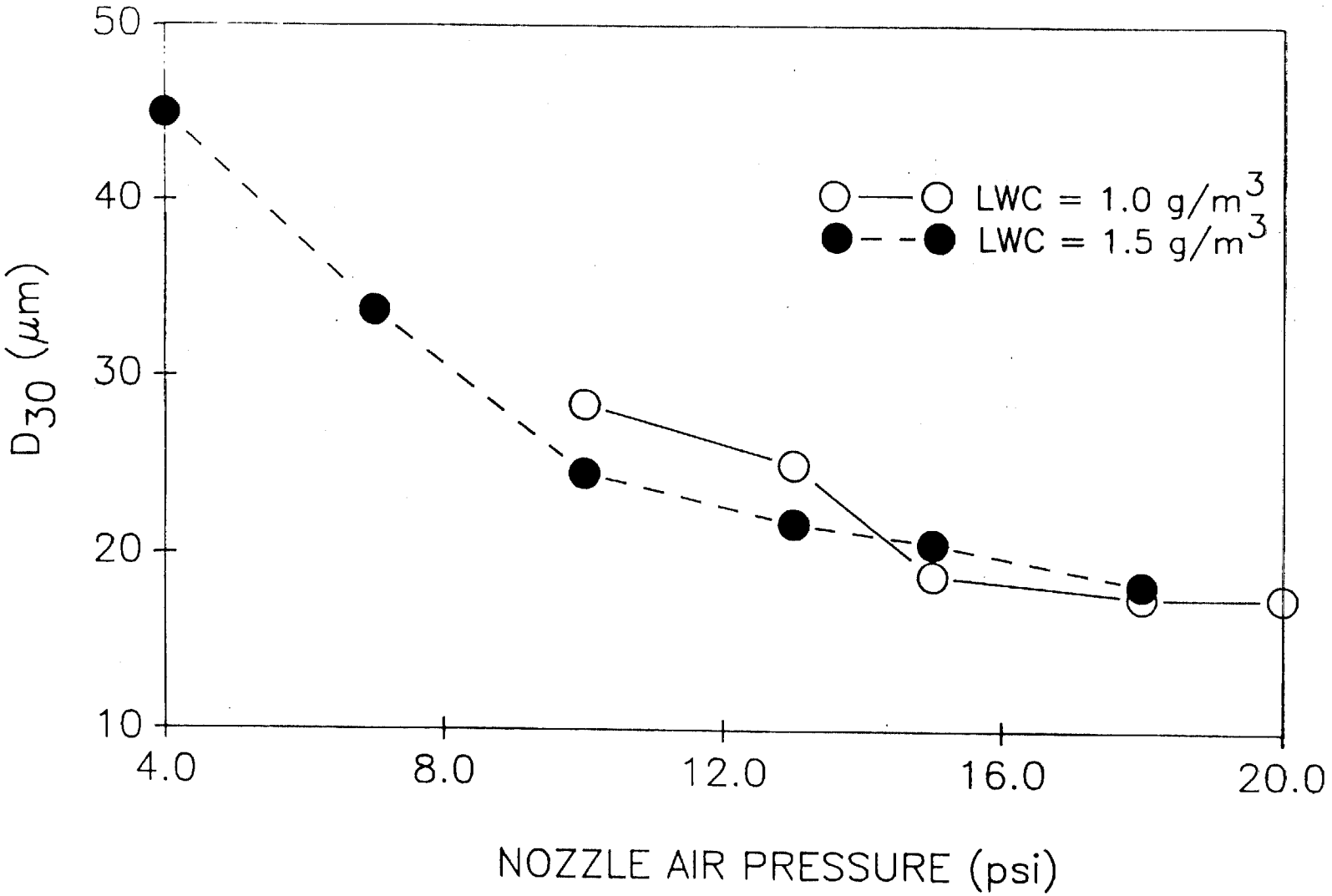

Figure 2.8 Volume Mean Diameter, D_{30}, Versus Atomizing Air Pressure

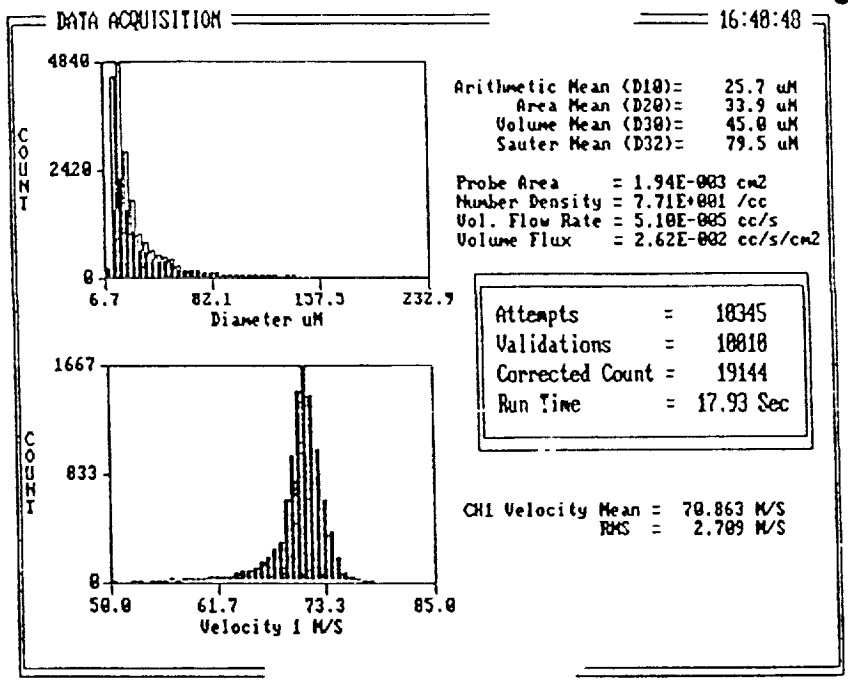

Figure 2.9 Size, Velocity, and Volume Distributions for LWC = 1.5 g/m^3

a) 27 kPa Atomizing Air Pressure

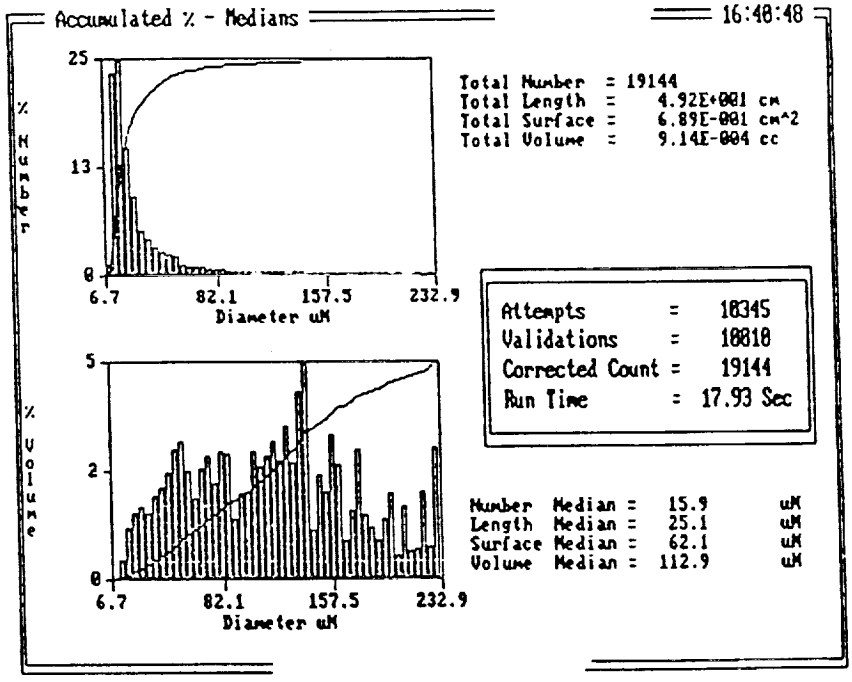

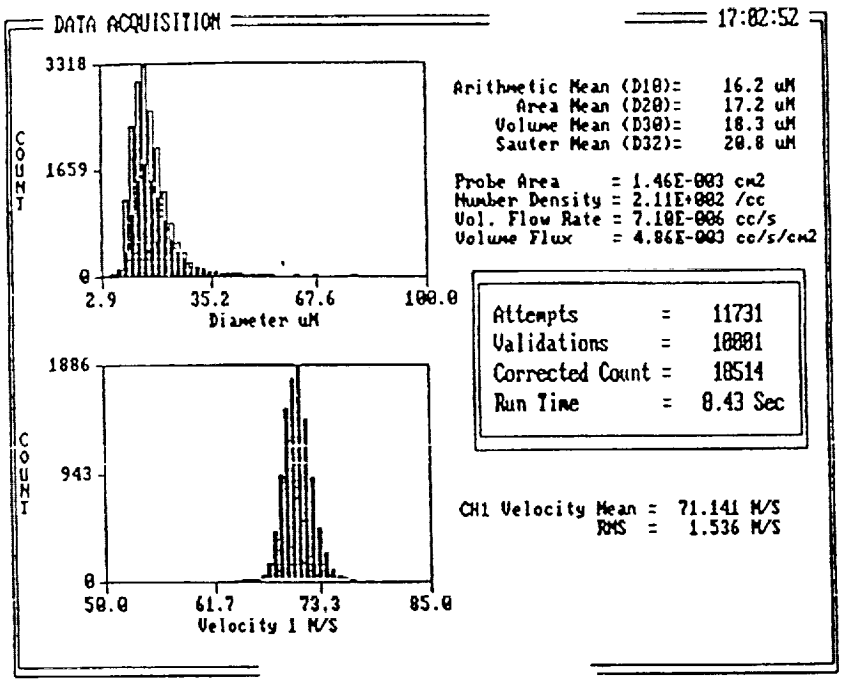

b) 124 Kpa Atomizing Air Pressure

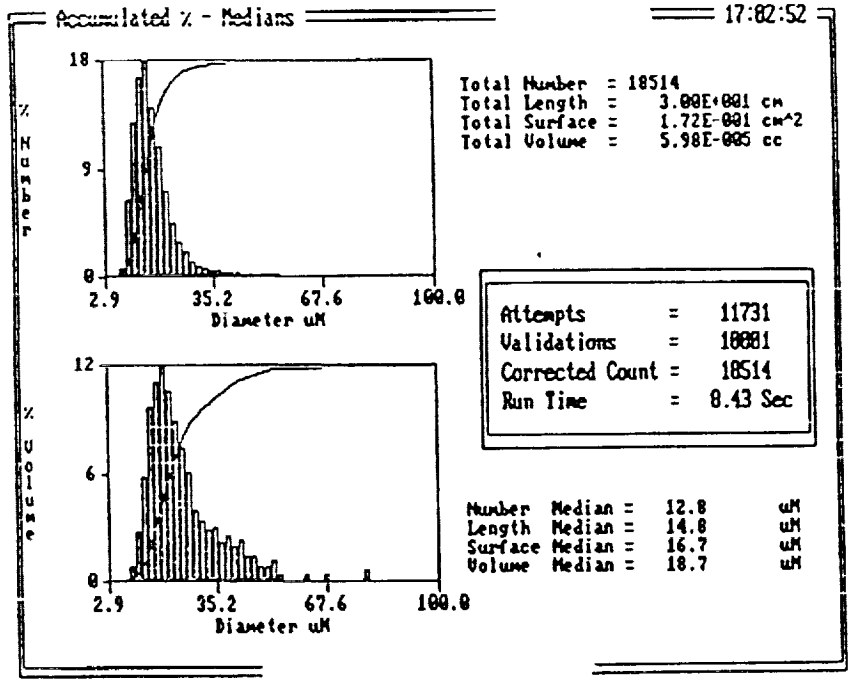

towards 20 um. This asymptotic behavior is characteristic of air-assist nozzles at high air to liquid ratios.[27] When the nozzle was atomizing more effectively at the higher pressures, figure 2.9b, there was a very small quantity of large drops. Therefore, by merely changing the atomizing air pressure a variety of clouds could be simulated with varying size spectra and number density.

Measurements were taken at only one point in the center of the test section. The LWC values measured with the PDPA for a series of atomizing air pressures are depicted in figures 2.10a and 2.10b for LWC's of 1.0 and 1.5 respectively. In examining the data, it is seen that excellent agreement to the theoretical values of LWC based on water flow, air flow, and the assumption of uniform spray distribution occur for the intermediate air pressures in both cases.

Unfortunately, the spray distribution in the test section apparently became non-uniform at the extremes of high and low atomizing air pressures. This was evidenced by the test section windows being completely ice-free at low atomizing air pressure, indicating a too high water concentration on centerline. In addition, the windows tended to ice very badly at the highest atomizing air pressure, indicating the spray was concentrated at the edges of the flow. Since measurements were made on centerline only, these non-uniformities explain the PDPA measurement variations. In the intermediate air pressure cases, icing

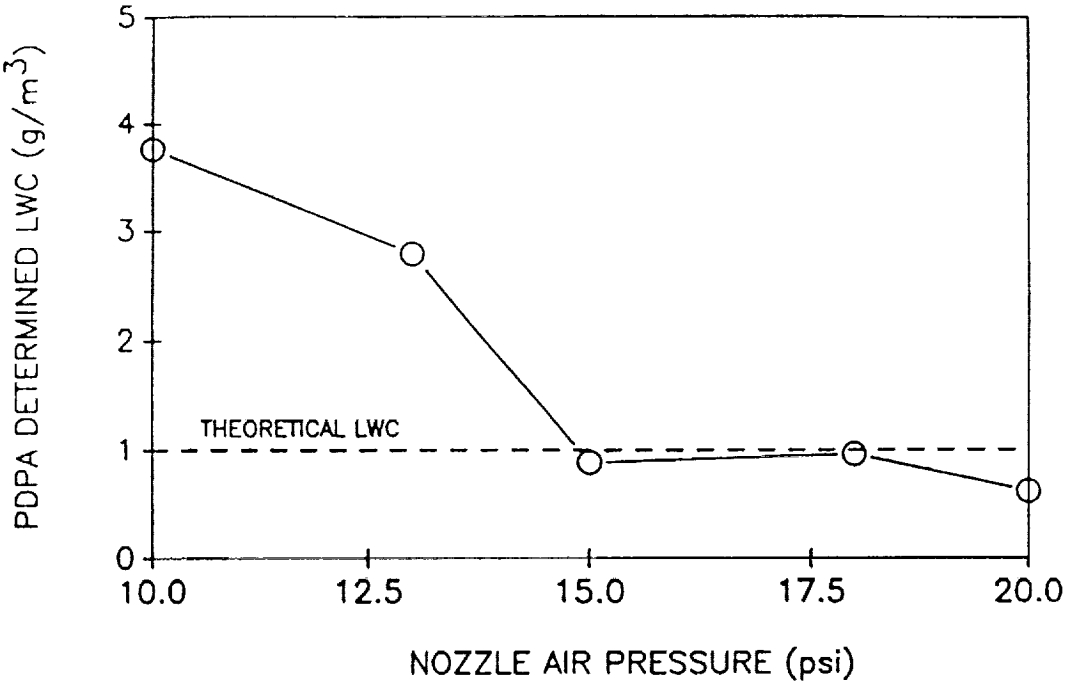

Figure 2.10 Liquid Water Content, LWC, Versus Atomizing Air Pressure

a) Nominal LWC = 1.0 g/m^3

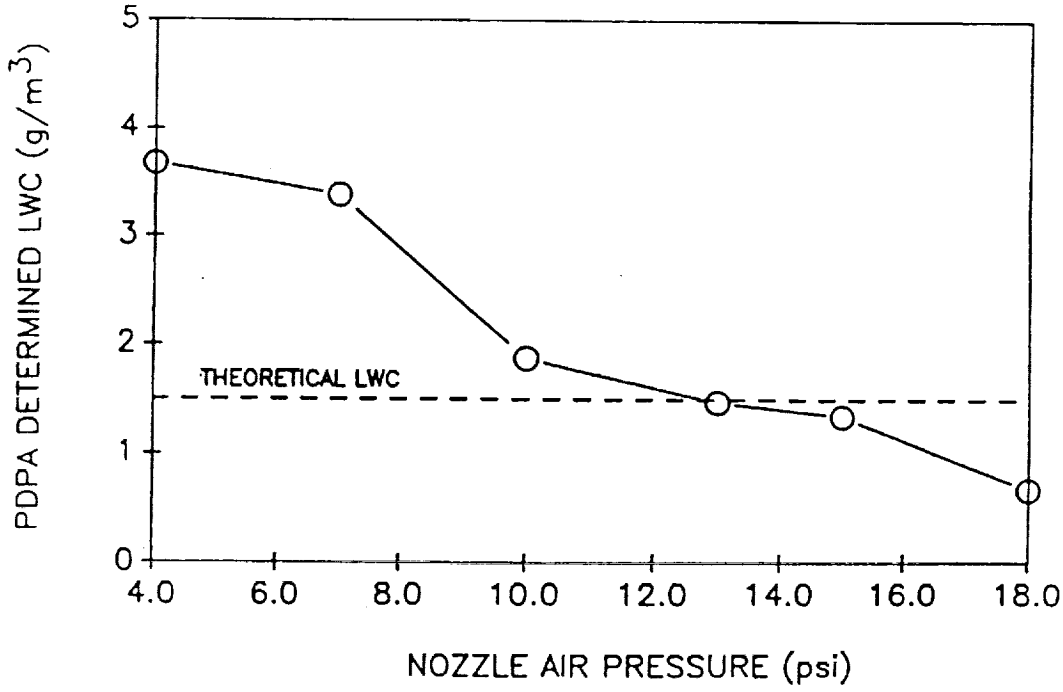

b) Nominal LWC = 1.5 g/m^3

was moderate, but not absent. Note that during the test the actual windows were heated to ensure no measurement errors due to ice accumulation could occur. A following section details the effects of window icing on the PDPA. Since nozzle spray characteristics such as spray angle and momentum can change tremendously when atomizing air-to-fuel ratio is altered, this non-uniform behavior is possibly understandable.

Overall, it was seen that the PDPA gave close to expected values of LWC under practical conditions in an icing tunnel. Further studies of this sort will require either ensuring that a complete profile of the LWC is taken across the test section to account for non-uniformities, or that more care is taken to ensure that spray distributions within the wind tunnel are more uniform.

Window effects

An important consideration when making optical measurements, whether with a compact optical probe or with a full size instrument is ensuring that any windows the instrument views through are kept sufficiently clean, dry and/or ice-free to prevent errors in the data. The ramifications of obscuration include beam steering of the transmitting optics along with attenuation of the received scattered light. If beam steering occurs the beams will not cross and measurements will be impossible. If attenuation occurs, the smaller particles which scatter less light are the first to be missed. Since these particles normally

occur in the greatest number in typical size distributions, errors in the number density can occur if these particles are missed.

There are a number of means for preventing these window obscuration problems. They range from heated windows for icing tunnels or in front of the instrument lenses in icing conditions, to blowing air in front of the windows to form an air curtain. The prototype fiber optic probe utilized hoods with purge air to keep droplets out. These hoods, seemed to work well in fogs and small diameter sprays.

The problems of window obscuration are therefore important to consider, but present primarily a mechanical design difficulty which can be met in a variety of effective means.

2.2 Fiber Optic Probe Development

A compact fiber optic probe has been developed by Aerometrics to replicate the success achieved by the standard PDPA in obtaining accurate particle size and liquid water content measurements. The advantage that such a device holds over its predecessors is that it has the potential of being lightweight, compact, robust, and waterproof. Hence, such a probe is well suited for measurements on an aircraft or in a large scale wind tunnel under varied conditions.

Figure 2.11 shows a schematic of the prototype fiber optic-based PDPA. This instrument was built in order to establish that a probe could be constructed that exactly

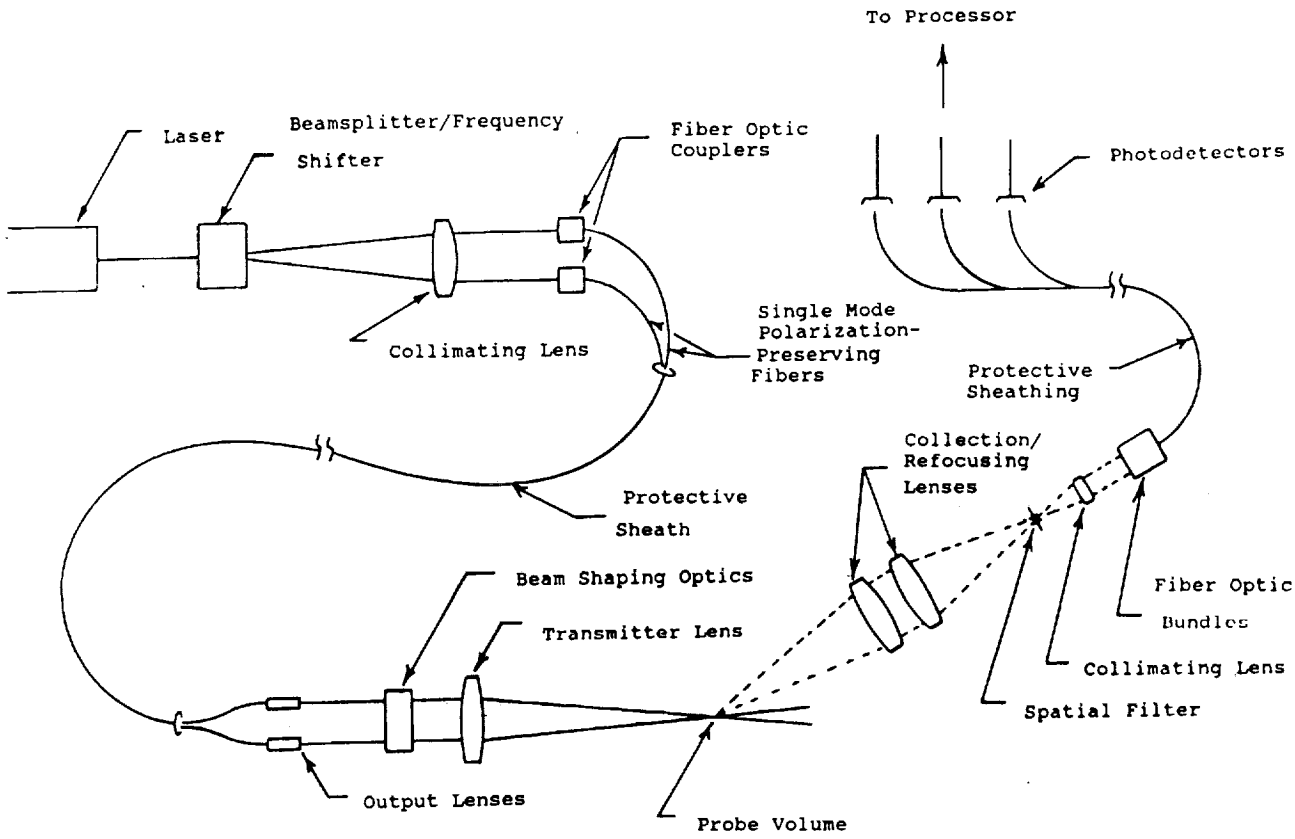

Figure 2.11 Fiber Optic PDPA Schematic

Fiber Type	Modal Birefringence B x 10^{-4}	Mode-Coupling Param. h x 10^{-6}/m	Loss @ 0.63 microns dB/km
Elliptical Core	4.2	30	85
Bow-Tie	6.7	42	< 12
Pit-in-Jacket	5.9	44	< 12

Table 2.1 **Properties of Typical Fibers**

duplicates the performance of the standard instrument. No special considerations were given to protecting such a device from the harsh environment found in aircraft icing research. To make the transmitter probe portable and rugged, the laser, beamsplitter and frequency shift unit is placed in a single package located outside the test environment. Two single mode, polarization-preserving optical fibers, one for each beam, lead to the transmitter probe head. In the probe head the beams are manipulated to produce the desired focused beam size and fringe spacing at the measurement volume. The receiver probe head is designed to collect scattered light emanating from the measurement volume using an F/3.3 cemented doublet lens. The collected light is refocused to a spatial filter to define the extent of the measurement volume and then coupled into a multimode fiber bundle. This receiver cable takes the collected light and separates it into the detectors, located outside of the test environment, for signal processing.

The most critical aspects in the design of the probe are the efficiency and effectiveness of the optical fibers and couplers used in the system. At the transmitter, single mode, polarization-preserving fibers must be used to provide the highest intensity and visibility of the interference fringes at the measurement volume. Furthermore, the couplers used to transmit the laser light into the fibers must optimize the transmission efficiency while maintaining alignment of the polarization axes of the fibers. Finally,

multimode fibers are to be used in the receiver to transmit the scattered light to the photodetectors. Such a fiber system must also be highly efficient and must have the ability to provide the necessary spatial frequency information used to obtain particle size. What now follows is a discussion of the aforementioned critical design issues.

2.2.1 Analysis and Selection of Single Mode Polarization-Preserving Optical Fibers

The PDPA method makes use of the interference pattern that results from the combination of two coherent, polarized laser beams. Such an application calls for the use of single mode, polarization-preserving fibers. A brief description of these fibers will serve to help one appreciate the difficulties associated with their use.

In a multimode fiber, there exists several different paths that a light ray may take through the fiber. This is mostly due to the large core diameter of the fiber, which is typically greater than 100 microns. If the core size is reduced, it will reach a point where only one path through the fiber is possible. The consequence of this is that all of the energy in a beam of light passing through the fiber will travel the same path. Modal dispersion is thus nearly eliminated, allowing highly coherent laser light to emerge with its critical properties unchanged. Such a fiber is called a single mode fiber. The optimum core size of a single mode fiber will vary with the wavelength for which it

is designed. A typical core size for visible light is 4 microns.

In order to maintain the polarization of the light within the fiber, the normal propensity of light to transfer between the two polarization states must be suppressed. This is accomplished by introducing a stress asymmetry creating high birefringence around the core. The small core size plus this stress asymmetry are the major features which make up the single mode polarization-preserving fiber.

Only recently has progress in manufacturing techniques reached a point to where such fibers have been commercially available. Such techniques have only been developed since 1980[28] , and even today there are certain limitations on the performance of commercial fibers. A review and analysis of the performance characteristics of single mode polarization-preserving fibers is therefore needed in order to understand the choices made for the PDPA probe.

In analyzing the properties of single mode polarization-preserving fibers, two important concepts are often encountered. They are: 1) the transmission efficiency of the fiber and 2) its ability to maintain the polarization of the transmitted light despite any environmental conditions that may exist outside of the fiber. Of the two, the second requirement is the hardest to achieve.

Two parameters that relate to the fiber's ability to maintain polarization are modal birefringence and the mode-coupling parameter. Modal birefringence, B, describes the

difference between the two orthogonal linear-polarization modes. It is an indication of the difference in the propagation constant between the two modes. Enlarging the modal birefringence is tantamount to improving the polarization maintaining characteristics of the fiber. The mode coupling parameter, h, is a measure of the fiber's ability to maintain its polarization based on random mode-coupling. This parameter is closely related to fiber cross-talk, which is the ratio of the optical power in the two radiated polarized modes, expressed in decibels. As h decreases, the modal coupling decreases.

Table 2.1 shows the tabulated values for three types of fibers.[29,30,31,32,33] The first is a typical example of a fiber with internal birefringence caused by the geometrical effect of the core. A large modal birefringence of 4.2×10^{-4} can be found in the elliptical core fiber. However optical losses of these fibers are generally high. The reason may be due to the large refractive index difference between the core and the buffer layer and the effect of imperfections in the core shape. The other two examples in the table are categorized as stress-induced birefringent fibers. These fibers exhibit low optical losses and low crosstalk by settling the buffer layer between the core and the stress-applying parts.

Similarities between the bow-tie configuration and the pit-in-jacket configuration justified an investigation to determine which of the two is most suitable for use in the

PDPA probe. Samples of both fibers were acquired and tests performed to analyze their polarization holding capabilities as well as ruggedness and ease in handling. The pit-in-jacket fiber proved superior in both its optical and mechanical properties. Herein reliability becomes a major issue in assessing fiber performance. On some lengths of the bow-tie fiber, minor flaws in the cross-section were discovered leading to increased environmental effect on the polarization state of the output beam. It is believed that such flaws occur due to the complicated nature of the bow-tie cross-section and equally complicated production requirements. The pit-in-jacket fiber has a simpler cross-section consisting of circular stress-applying parts. This minimizes the potential for deformation of the stress-applying parts as the fiber is drawn. Mechanically, a rugged nylon coating around the pit-in-jacket fiber provides for the much needed strength and abrasion resistance that the bow-tie configuration does not.

2.2.2 Methods of Coupling

Of almost equal importance to finding a fiber with low transmission loss and high birefringence is to devise a technique to couple the light from the laser into the fiber that minimizes insertion loss. This problem is aggravated by the extremely small cross-section of the single mode fiber and the need to orient the stress-applying parts of the fiber to correspond to the polarization state of the laser. With fiber diameters from 3 to 5 microns, a

positioning system with a resolution in fractions of microns is needed for maximum coupling efficiency. The task is further complicated by the small angle of incident light that can be coupled into the fiber. This angle is normally presented as the numerical aperture of the fiber and is typically 6 degrees.

At the present time three different methods are being used to resolve these difficulties. In the first technique ultra-fine precision linear and angular positioners are used to position the fiber in a focussed beam. A small amount of the light collected by the fiber is directed to a light sensor and multi-axes feedback system. This microprocessor controlled interface allows constant repositioning of the fiber to maximize the transmission efficiency. Such dynamic systems are bulky, extremely expensive, and may prove advantageous only for those applications where the tracking of wandering laser beams makes the following two methods unfeasible.

The second method commonly used is to simply position a polished end of the fiber into a highly focused beam. Much like the previously mentioned technique, this one commonly uses three dimensional linear translators along with two dimensional angular adjustment. The necessary resolution is usually provided by piezoelectric positioning devices or differential micrometers. The technique has proven successful in providing over 50% transmission efficiency into the fiber. The disadvantage of this method is again

the cost and size. Although they give a resolution of down to 0.1 micrometer, most systems utilizing this technique are designed for breadboarded laboratory experimentation. They therefore do not apply themselves well to the development of rugged portable laser instrumentation.

The third technique makes use of gradient index lenses. Whereas conventional lenses image light by the discrete refractions at the boundary of the lens material and the surrounding medium, gradient-index lenses consist of a cylinder of refractive material whose index of refraction varies in such a way as to make it possible to form images by continuous refraction within the lens material. Most gradient-index lenses are produced with a refractive index that varies radially within the lens.

The advantages of these lenses over conventional lenses are numerous. The most important advantage as it applies to optical fibers is that it allows a polished end of the fiber to be bonded to a face of the lens in such a way as to collect most all of the light incident on the opposite face.

One example of this method is pictured in figure 2.12. A collimated beam is incident on the face of the gradient-index lens. This lens, with the fiber attached, is allowed to tilt about its center axis. This tilt movement allows the focal point of the incident beam to fall upon the face of the fiber, yielding efficiencies of up to 75% for single mode polarization-preserving fibers. This technique has the added advantage of being compact, inexpensive, and rugged.

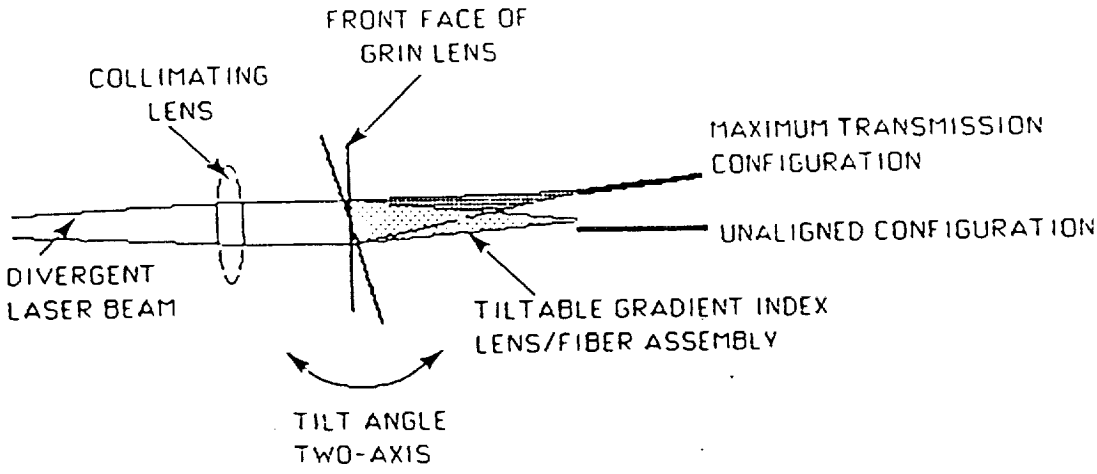

Figure 2.12 Axially Tilt-Adjustable Fiber Optic Coupler

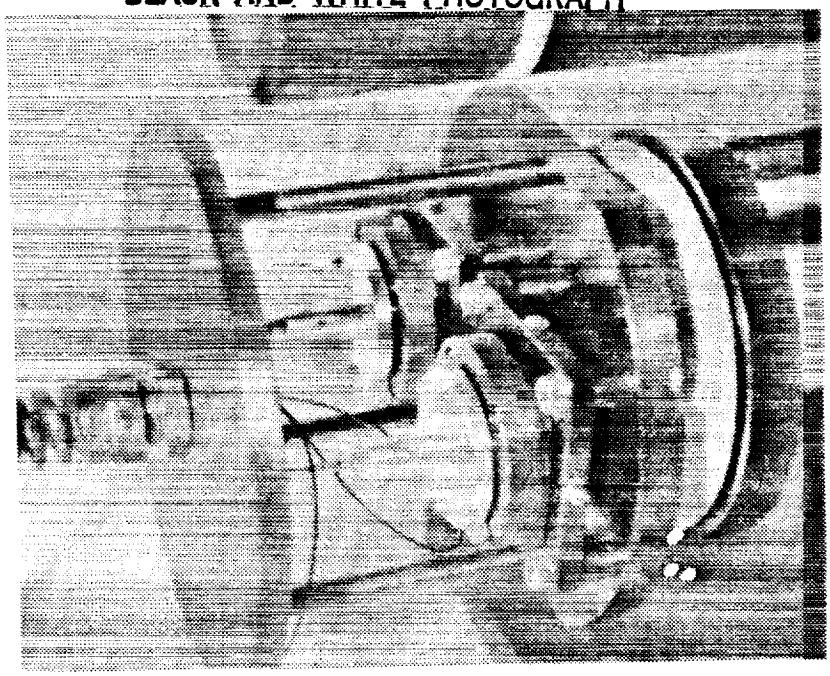

Figure 2.13 Prototype Single Mode Polarization-Preserving Coupler

This is mainly due to the fact that there are a minimum of moving parts, and the lens itself is lightweight and bonded to the end of the fiber.

A preliminary investigation into the above coupling techniques led to the acquisition of a gradient-index lens based coupler for the PDPA fiber optic probe. This prototype coupler is shown in figure 2.13. Tests with the coupler have been successful in coupling nominally 65% of the incident beam into the fiber, with at least 95% polarization maintenance.

2.2.3 Analysis and Selection of Multimode Optical Fiber Receiver System

The final development requirement to present itself is the problem of transferring the light collected by the receiver to the three photomultiplier tubes located at a large distance from the test region. Unlike the previously mentioned design challenges involving single mode fibers, the detection system utilizes standard multimode fibers for which the technology is already highly developed.

Minimization of coupling losses is again critical, for if loss is high then light scattering due to smaller particles (which scatter low intensity light) may not be detected, causing a bias towards the larger particles.

Research has been carried out for possible solutions to this problem. Two possibilities seemed feasible. The first makes use of fiber bundles to collect over the entire cross-section of the accumulated light. Fiber bundle technology

has progressed to a level where it has become a successful and moderately inexpensive method for gathering light. Its success may be based on two major advances. The first is the development of inexpensive low-loss fibers as the transmitting medium. This is an important breakthrough since many fibers are used in the typical bundle. As an example, for a 4 mm diameter circular bundle, about 250 fibers are needed. The second advance is the minimization of the non-transmitting portion in the cross-section of each fiber. Fibers that are placed in bundles presently have a core-to-fiber area ratio of up to 80%. This allows for coupling efficiencies of 60% or more.

Another option for collecting the scattered light once again makes use of gradient-index lenses to direct light into each fiber. In this case, only three highly efficient multimode fibers travel the distance from the receiver to the photodetectors. Each of the three fibers can then be positioned with their output ends in front of the photodetectors such that all of the light emitted from the fiber will be detected. The theoretical efficiency of such a system is 64%.

Both systems appear to present the highest coupling efficiencies available. An investigation was carried out to determine which method was the most desirable. Among the other factors to be considered were the cost (the gradient-index lens system being much less expensive, especially for longer lengths), ease of production, and ruggedness.

Sample cables were manufactured using each method. Each cable was 10 to 15 meters in length and connected the receiver to a set of photomultiplier tubes, pictured in figure 2.14. The results of the investigation indicate that the fiber bundle technique is superior in its performance for the following reason. In an optical system such as that in the receiver, slight deviations from the optimum alignment orientation can cause distortions in the normally circular cross-section of the collected light just before it's coupled into the fiber optic cable. Such distortions can be due to spherical aberration in the lenses or a knife edge effect of the edge of the spatial filter on the focused blur spot. Spherical aberration may be remedied by evaluation and redesign of the lenses that collect and refocus the light. The knife edge effect which occurs when the focused blur spot is approximately the same order of magnitude as the width of the slit can also be attributed to poor lenses. However, this effect may also be caused by the magnification ratio of the collection and focusing lenses. If for example the focal lengths of both lenses are the same then the resulting image at the spatial filter will be the same size as the source spot. This spot size is a function of the diameter of the particle which scatters the light. For particles with diameters greater than 100 microns the magnification ratio can indeed be a factor hindering the performance of the lens system.

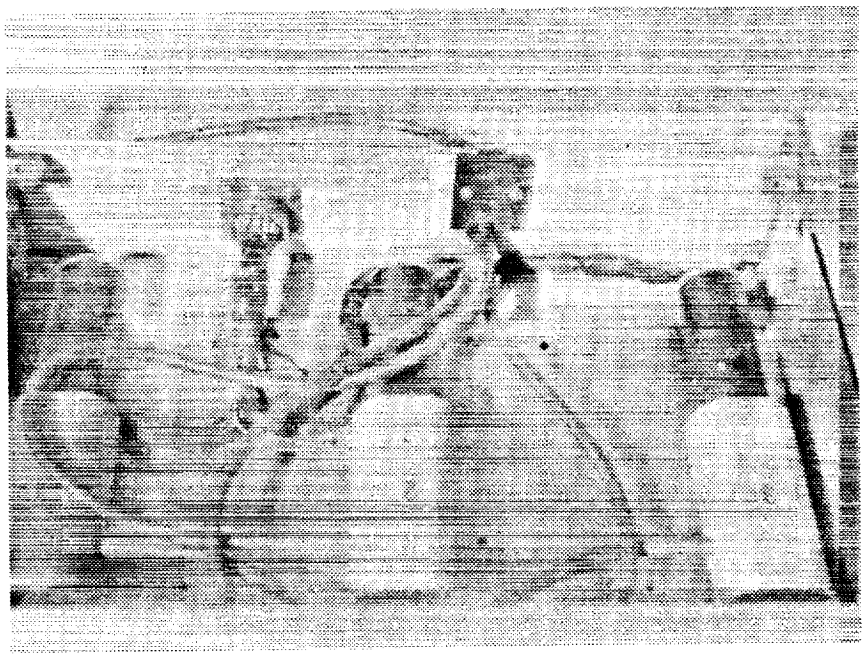

Figure 2.14 Multimode Fibers Coupled to Photomultiplier Tubes

Tests using the gradient-index lens configuration displayed the effects of this distortion. In some instances, scattered signals could be observed on all but one of the three channels. The quality of the observed signals also varied considerably as the alignment of the receiver was changed slightly. Focusing of the receiver to make the blur spot at the spatial filter as small as possible became a major task, and slight variations (less than 0.5 mm) of the position of the receiver from the ideal focused position caused major signal distortion.

Since the choice of lenses in the receiver must necessarily be governed by collection efficiency and lens availability, the magnification ratio must be treated as invariant. In view of this, the fiber bundle configuration emerges as the best method. This is mostly due to the fact that there are multiple fibers for each of the three detectors, rather than just one. Therefore, the possibility of total loss of signal in one of the channels is extremely slight. The knife-edge effect previously mentioned would only result in a lower signal amplitude in all three channels, rather than a total loss of signal in one or more channels.

2.3 Fiber Optic Probe Configuration

All of the previously mentioned fiber optic techniques have been incorporated in the building of a prototype PDPA transmitter and receiver. The assembled probe is pictured in figure 2.15. The mounting arm that supports the

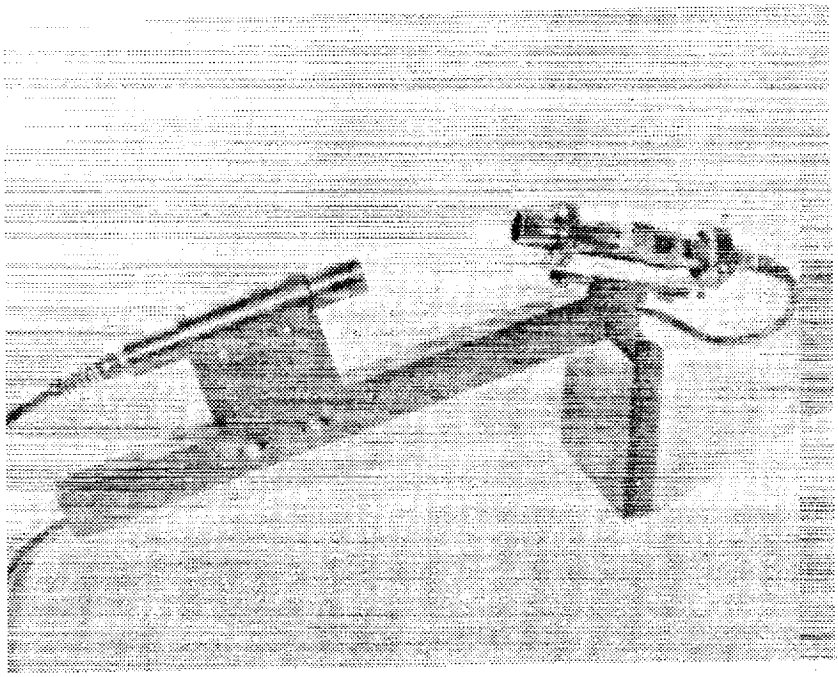

Figure 2.15 Fiber Optic Probe - 30^{o} Forward Scatter Configuration

transmitter and receiver serves the dual purpose of rigidly supporting both probe heads as well as providing all of the necessary adjustment used in the alignment of each. It has been designed to accommodate the full range of optical parameters that may be used, and can be modified to a more compact design for use in a measurement environment where information on the particle size and velocity range is known.

A sketch of the transmitter structure is shown in figure 2.16. In designing the transmitter, much thought went into designing a single product than can accommodate a variety of particle size and velocity ranges. This has been accomplished by modularizing each primary function within the transmitter. The "transmitter modules" are optical packages whose duties are to change the spacing between the two beams and to change the individual beam diameters before they are brought to focus by the transmitter lens. The end result of switching from one module to the other is to change the measurement volume size and the fringe spacing, allowing the user to change from one size and velocity range to another. The second modular component used in the transmitter is the transmitter lens itself. The effect of changing this lens is to also change the fringe spacing and measurement volume size.

Both the lens and the transmitter module are enclosed in a 28.5 mm cover which is o-ring sealed to prevent the entry of moisture. The lens is protected by a optical

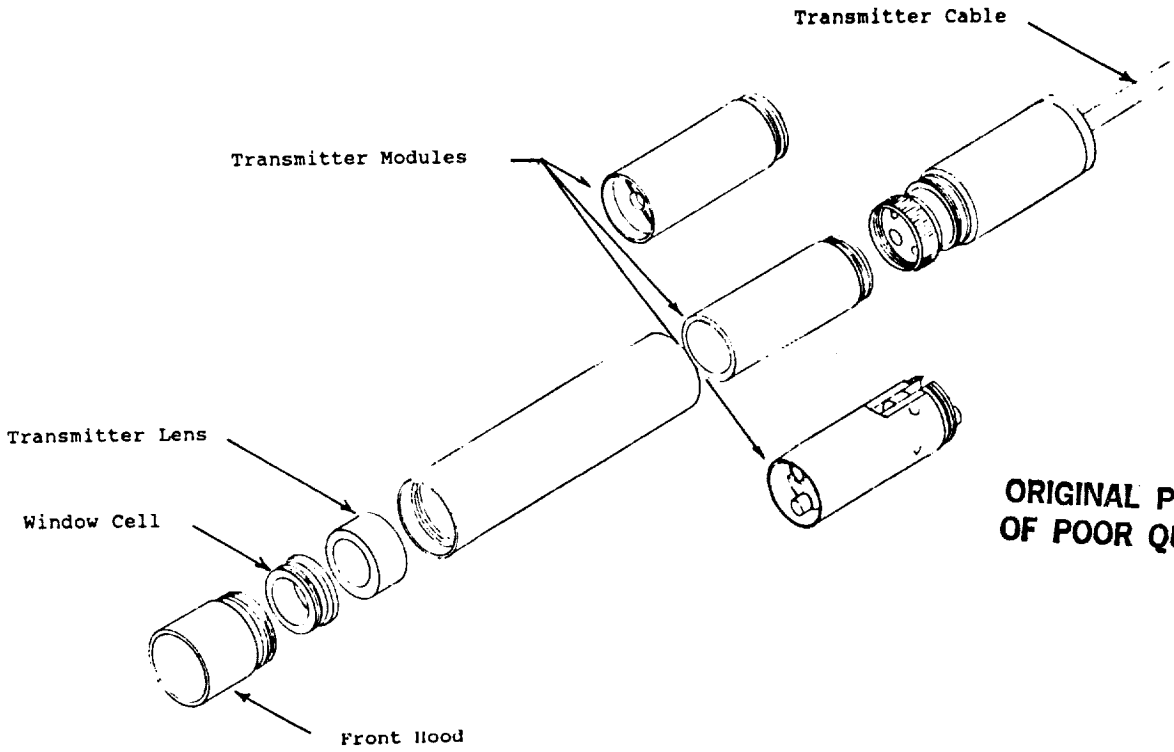

Figure 2.16 Transmitter Probe Exploded View

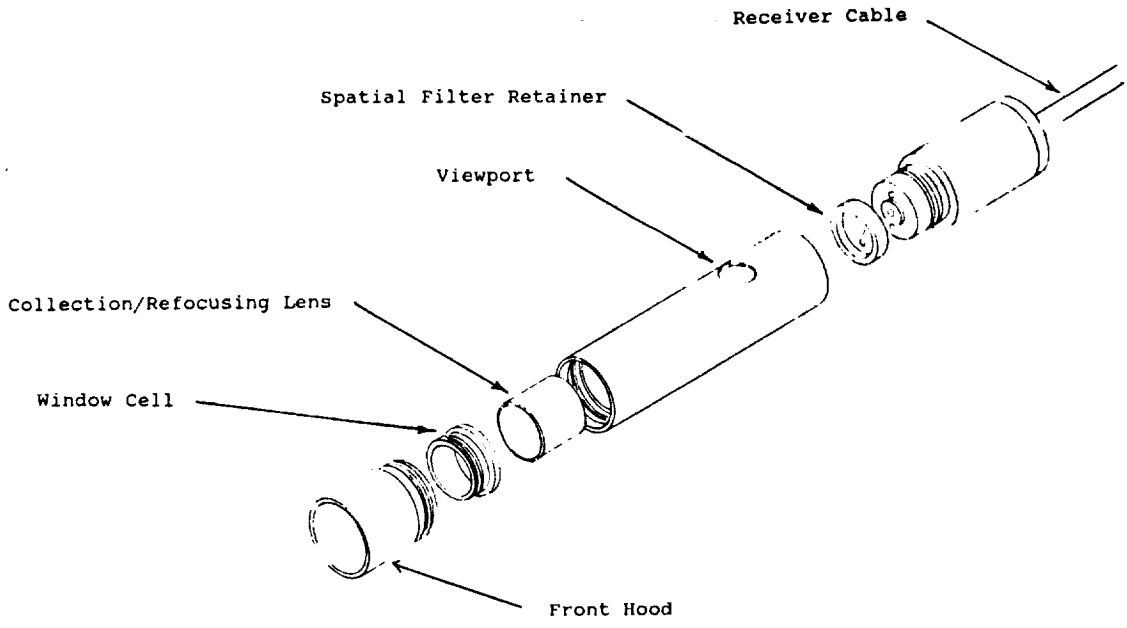

Figure 2.17 Receiver Probe Exploded View

quality coated glass window, which can be removed and cleaned when necessary.

The prototype receiver, which was built following the basic design of the standard receiver, is shown in figure 2.17. As in the transmitter, the receiver probe is designed for versatility. Once again the modular nature of the receiver probe allows the user to change the collection lens or the size of the spatial filter to suit the characteristics of the particle field being measured. For example, for dense sprays composed of small (1 to 30 micron) particles a 60 mm collection can be used with a 50 micron spatial filter slit. This reduces the size of the portion of the measurement region that is seen by the detectors and thus reduces the incidences of scattered signals from two independent events combining to form one extended burst.

The receiver lens is also covered by a glass window to prevent the entry of water. The entire package is o-ring sealed for the same reason. A further measure is taken to prevent contamination of the windows by water droplets. If water does build up on the windows it can distort the path that the light takes through the system. This results in a reduction, if not total elimination, of the instrument performance. To inhibit this droplet buildup inserts have been designed to run purge air across the window and out of the front openings of both the transmitter and receiver.

Listed in table 2.2 are the combinations of optical parameters that affect the size and velocity range

LASER WAVELENGTH 0.6328 microns
LASER BEAM DIAMETER 0.68 mm. (to 1/e^2)
30 DEGREES FORWARD SCATTER (slope = 0.7614)

BASED ON ESTIMATED VALUES ONLY

TRANS. MODULE	TRANS. LENS FOCAL LENGTH (mm)	BEAM SEPARATION (mm - approx.)	FOCUSED BEAM WAIST DIA. (microns)	FRINGE SPACING (microns)	NOMINAL FRINGE COUNT	MAXIMUM VELOCITY w/o OFFSET m/s (1)	STANDARD RCVR LENS: 100 mm DIAMETER MIN (microns)	STANDARD RCVR LENS: 100 mm DIAMETER MAX (microns)	OPTIONAL RCVR LENS: 60 mm DIAMETER MIN. (microns)	OPTIONAL RCVR LENS: 60 mm DIAMETER MAX (microns)
none	100	14	134	4.5	30	90	0.8	131	0.5	79
	200	14	269	9.0	30	181	1.6	262	1.0	157
	300	14	403	13.6	30	271	2.5	394	1.5	236
1/4 : 1/4	100	4	537	18.1	30	362	3.3	525	2.0	315
	200	4	1074	36.2	30	723	6.6	1050	4.0	630
	300	4	1611	54.2	30	1085	9.9	1575	5.9	945
1/4 : 1	100	14	537	4.5	119	90	0.8	131	0.5	79
	200	14	1074	9.0	119	181	1.6	262	1.0	157
	300	14	1611	13.6	119	271	2.5	394	1.5	236

1 20 MHz processor limit

Table 2.2 Parametric Table for PDPA Fiber Optic Probe

capability of the instrument. As mentioned previously, these parameters are the transmitter lens, transmitter module, and the receiver lens.

The overall dimensions of the assembled probe is roughly 24 inches long by 6 inches high and about 3 inches in width. The assembly weighs 6 lbs. All cables are covered with a PVC coated, steel coil reinforced protective sheathing.

2.4 Fiber Optic Probe Evaluation

Preliminary investigative tests were performed on prototype version of the fiber optic probe. Of primary interest are the following:

1. Demonstrate the total and dynamic size range. Quantify upper and lower limits and compare with the standard PDPA.
2. Evaluate number density measurement capabilities. Compare with the standard PDPA and to line-of-sight beam extinction using the Lambert-Beer law.
3. Evaluate mass flux measurement capabilities. Compare with standard PDPA and to direct sampling.
4. Investigate the effect of ice crystals on measurement. Perform tests with NaCl as a simulated ice crystal and with spherical particles or droplets to investigate the ability of the instrument to reject those scattering events caused by crystalline substances.

The above items 1 through 3 were evaluated in simultaneous measurements made on a 3 gph solid cone

pressure atomizer by the probe and the standard system. The nozzle operated at a pressure of 60 psi. Data was taken at three different axial positions Z = 57, 72, 98 mm below the nozzle. 5 mm radial increments across the spray were measured at each axial height. The results of the intercomparison are discussed below.

2.4.1 Intercomparative Study Between the Standard PDPA and Fiber Optic Probe

The first item of interest in this intercomparison is the establishment of the accuracy of the sizing capabilities of the probe. Before any tests were made with the pressure atomizer, simultaneous measurements were made on a ultrasonic drop generator to demonstrate the probe's ability to measure very small particles. The results are very important because such a test can quickly show whether optical losses in coupling light into the fibers are excessive, and whether the measurement system is biased towards the larger particles. As the results show in figure 2.18, the agreement between the standard system and the probe is excellent.

Figure 2.19 shows the size measurement results of the intercomparative study carried out on the pressure atomizer. In these graphs the arithmetic mean (D_{10}) and the Sauter mean (D_{32}) are plotted at various stations across the spray. From these graphs one can see the following trends. First, the fiber optic probe consistently measured a slightly smaller mean diameter than the standard instrument.

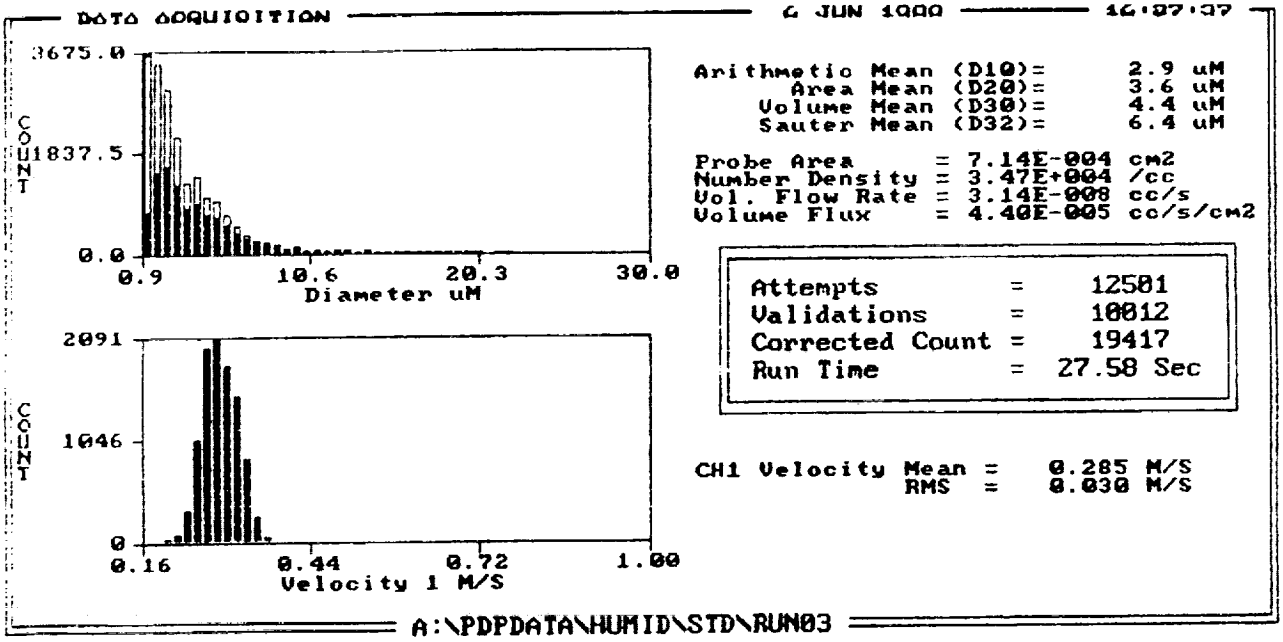

Figure 2.18a Size and Velocity Histograms Using PDPA - Ultrasonic Droplet Generator

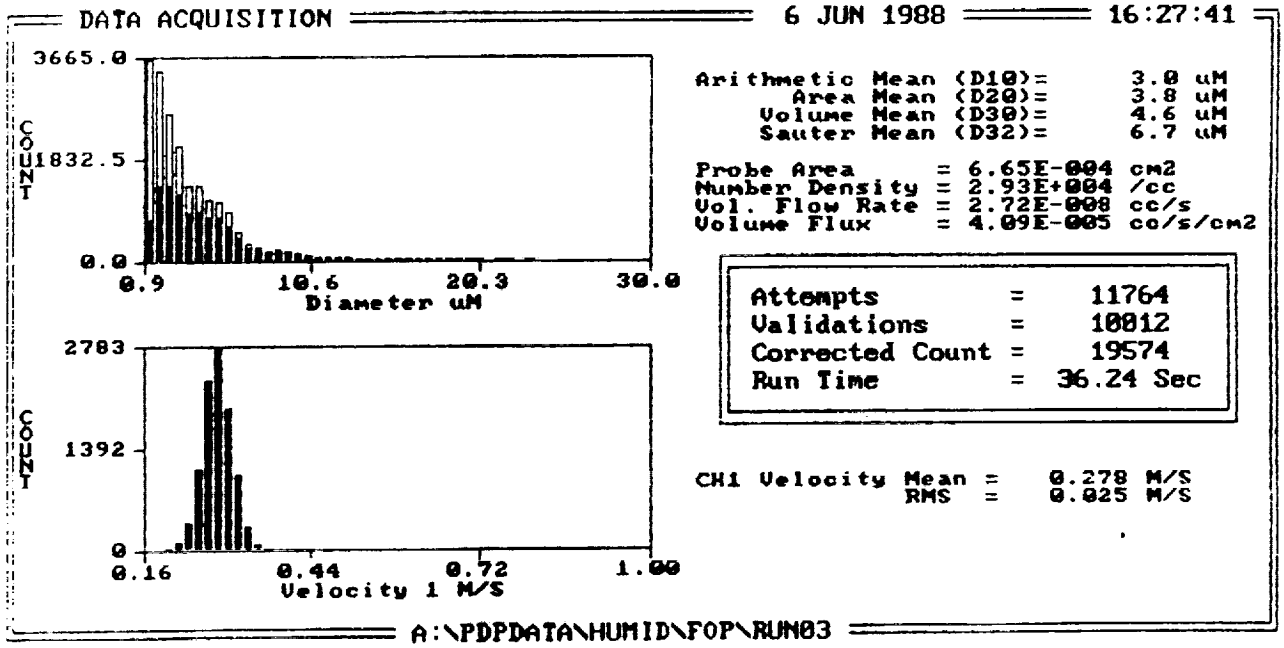

Figure 2.18b Size and Velocity Histograms Using Fiber Optic Probe - Ultrasonic Droplet Generator

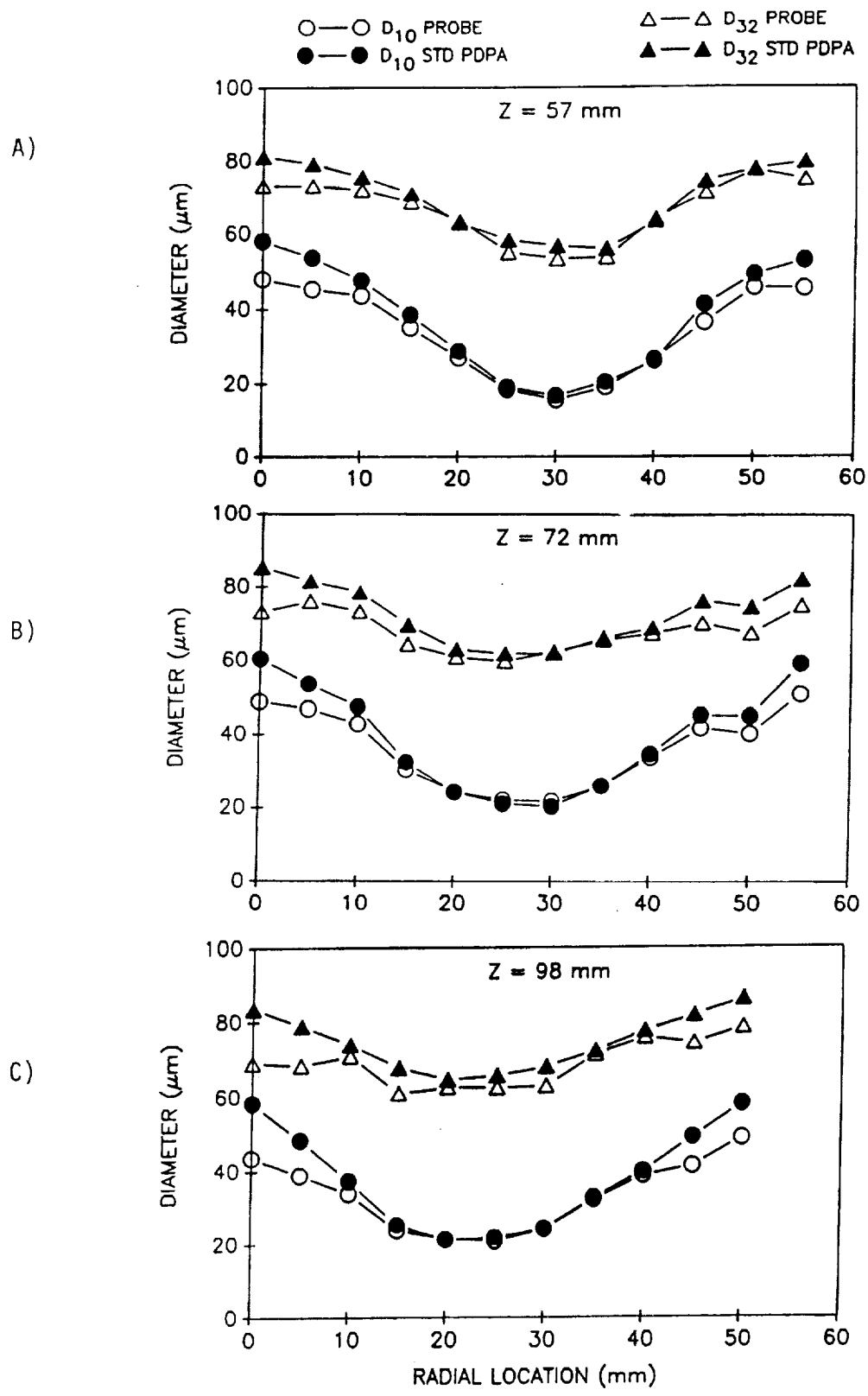

Figure 2.19 Radial Profile of D_{10} and D_{32} for Fiber Optic Probe and Standard PDPA

a) Z = 57 mm
b) Z = 72 mm
c) Z = 98 mm

Secondly, the mean diameters agree quite well in the center of the spray while tending to differ by up to 15 percent on the edges of the spray field.

This discrepancy is quite possibly due to the effects of oblique trajectory of the particles at the edge of the spray through the probe volume. In order for the probe volume correction to work properly, a physical measurement of the probe volume size is performed during data acquisition. This measurement (for a single component instrument) is dependent upon the average flow angle of the spray being orthogonal to the fringe pattern. Clearly, the probe and the standard PDPA show some differences in their sample volume correction response to oblique trajectories.

This matter has no consequences at all in the application of the probe to icing research, since the average flow angle in a wind tunnel or on an aircraft is generally very close to perpendicular to the plane of the fringes in the measurement volume. Thus in the most representative region of the spray, which is the center, the agreement is excellent.

The next issue to be addressed by the intercomparative study is the investigation of the measurement of number density by each system and the comparison of these results with extinction measurements made in the spray. Because of constraints on the geometry of the test facility, the actual extinction comparison had to be carried out with the probe alone. Sufficient data was however taken with the standard

system to make generalizations in the performance of both instruments.

The results of the simultaneous measurement of the number density in the spray at various locations are shown in figure 2.20. On all three plots one can notice a systematically larger number density measurement made by the probe. This is consistent with the results of size measurement, where it was noticed that size measurement for the fiber optic probe was slightly smaller. As is shown in figure 2.21, which displays a typical simultaneous measurement by the standard and fiber optic PDPA, the smaller sizes account for most of the total population of droplets in the spray. Thus, one would expect that the instrument which measures the smaller size would also measure the larger number density. In the center of the spray this difference is less than 20 percent. Using the same logic that accounted for the higher number density, one expect to see less of a difference in the measurement of mass flux, which is dependent on the volume of the measured particle size and thus influenced primarily by the larger particles in the size histogram. This will be discussed shortly.

The experimental arrangement for performing the line-of-sight measurements on a spray nozzle is shown in figure 2.22. The nozzle used was a Parker Hannifin air-assist research nozzle. Tests were performed at two axial distances from the nozzle. Both tests were carried out

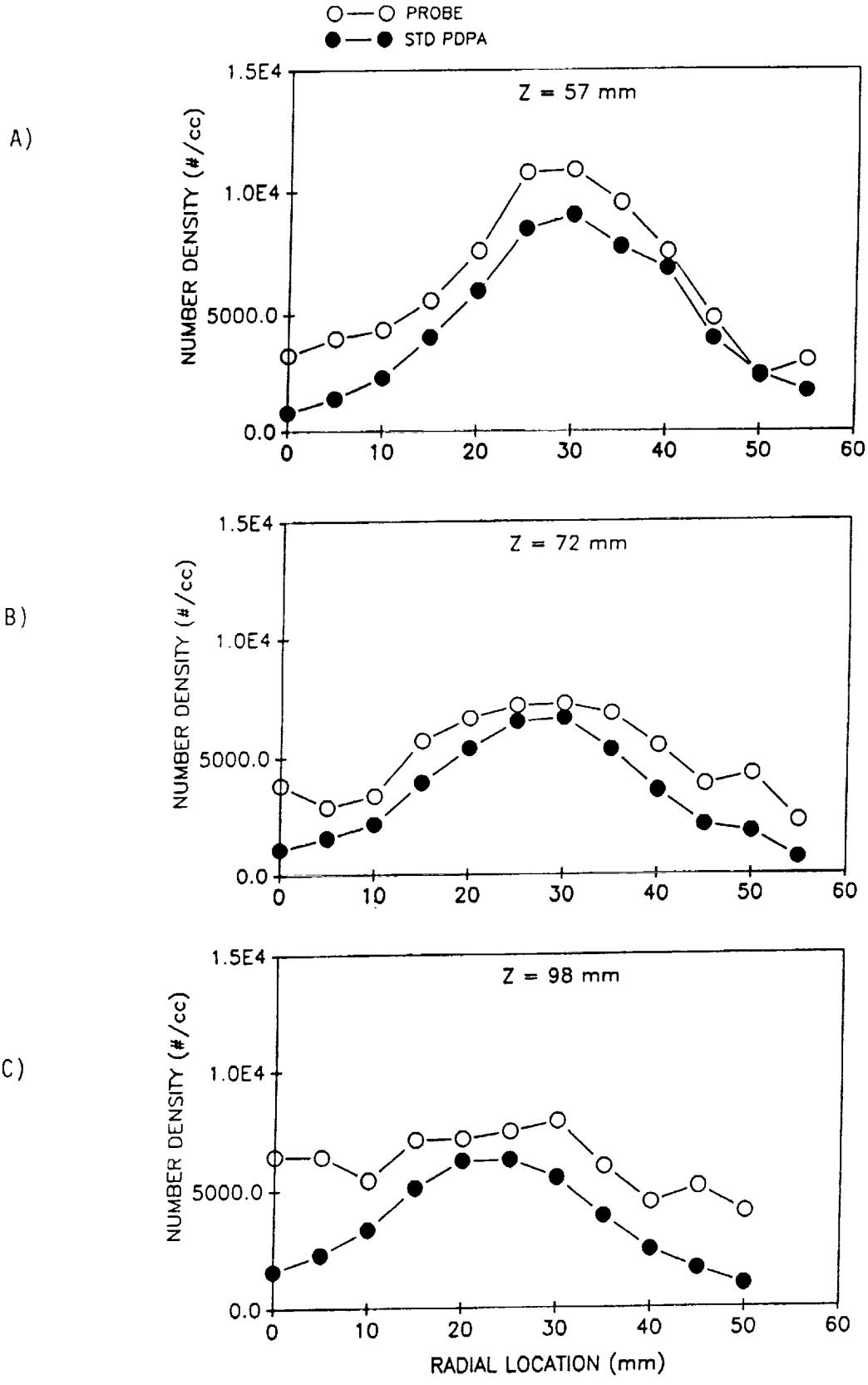

Figure 2.20 Radial Profile of Number Density for Fiber Optic Probe and Standard PDPA

a) Z = 57 mm
b) Z = 72 mm
c) Z = 98 mm

A)

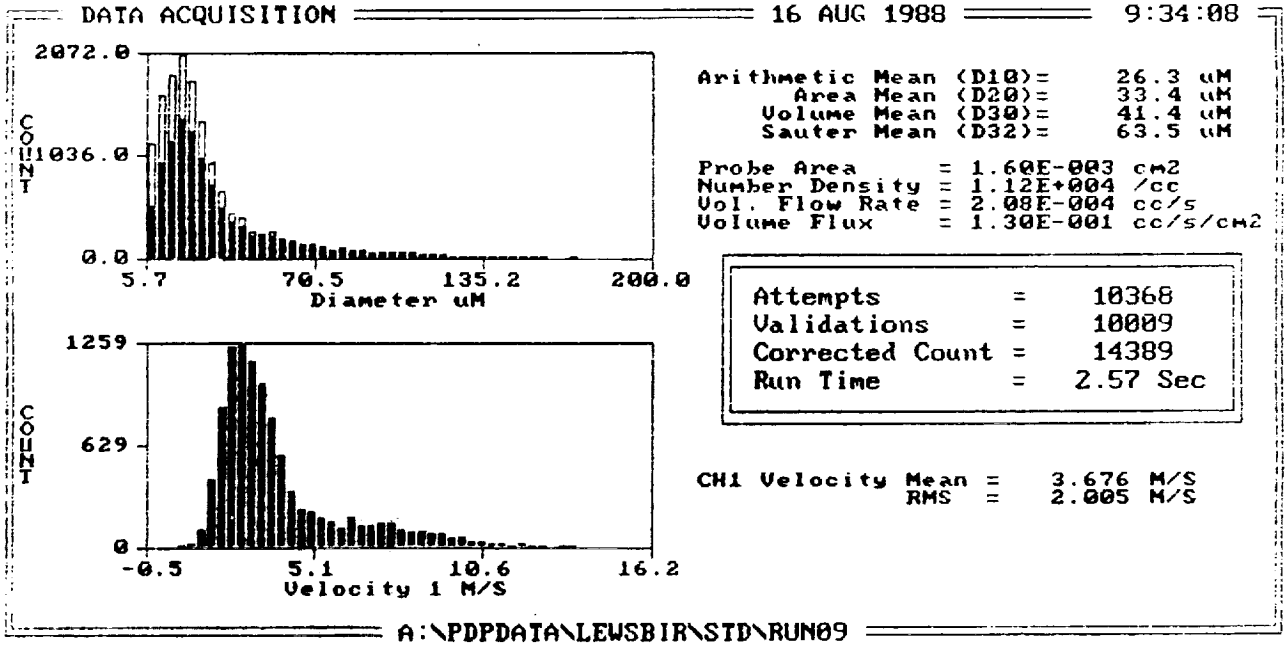

B)

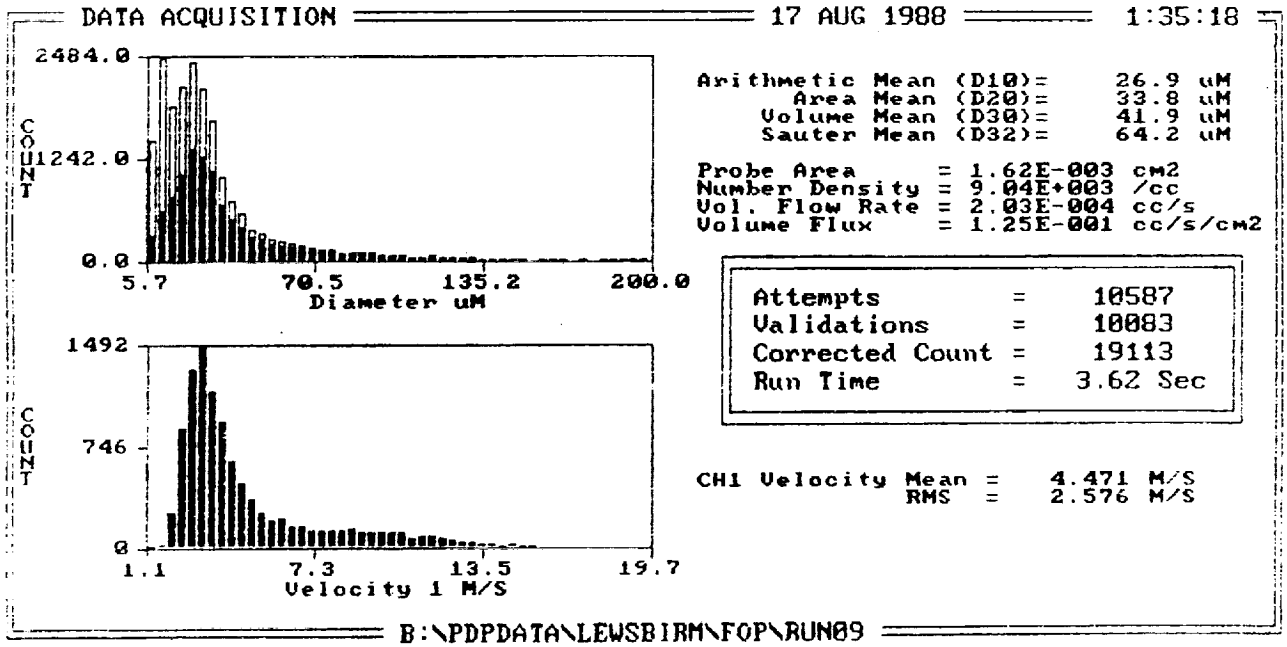

Figure 2.21 Simultaneous Measurement of the Pressure Atomized Spray
a) Standard PDPA
b) Fiber Optic Probe

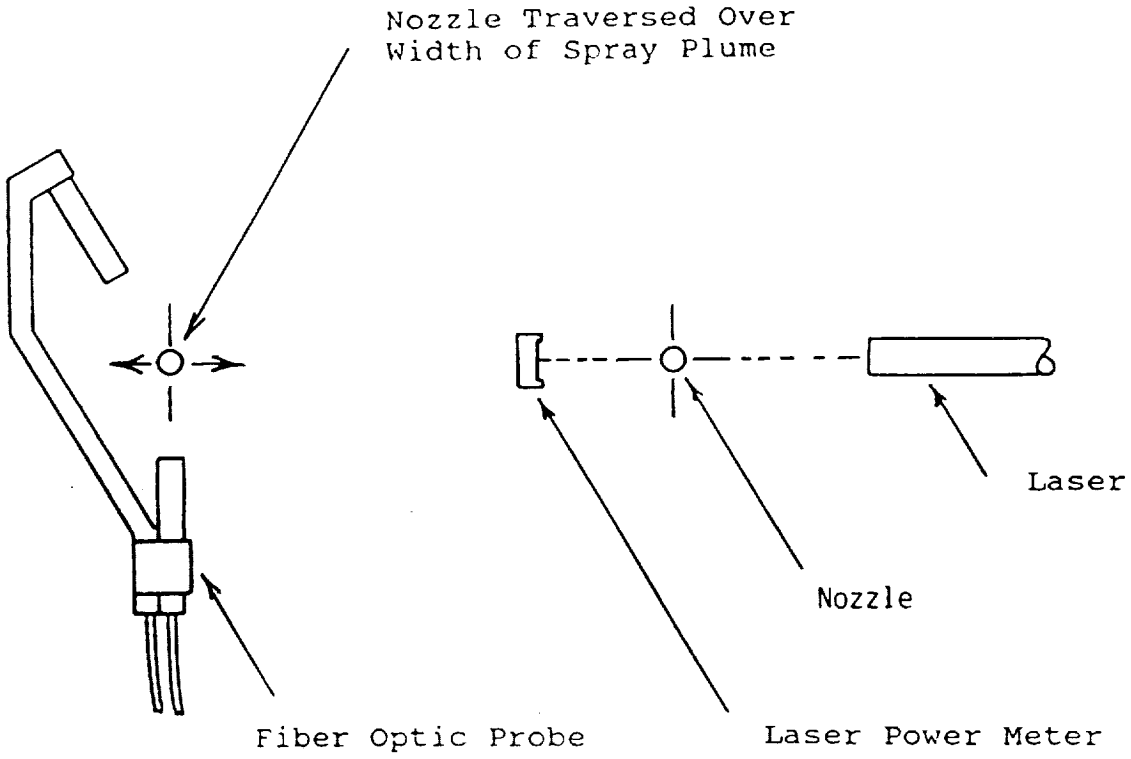

Figure 2.22 Experimental Arrangement for Extinction Measurement (right) and Using PDPA Probe (left)

Axial Position cm	Transmittance Extinction System	PDPA Probe	Percent Difference
5.0	0.692 +/- 0.016	0.651	5.9
10.0	0.667 +/- 0.026	0.518	22

Table 2.3 Comparison of PDPA Probe and Extinction System Transmittance, Parker Hannifin Research Nozzle

using a 415 kPa water pressure and 13.8 kPa atomizing air pressure. Measurements were taken at 5 mm radial intervals across the spray and optical transmittance calculated using the Lambert-Bouger or Beer's Law.

A comparison of the results obtained using extinction and Beer's Law is shown in table 2.3. Good agreement can be seen at both axial distances. The systematically lower transmittance derived from the probe measurement can be accounted for by the observation of the probe's systematically larger number density measurements compared to that of the standard instrument. The deviation of the transmittance is consistent with the magnitudes observed in comparing the number density measurements between the two systems.

The final parameter to be compared is the measurement of the mass flux. As was earlier noted, one would not expect a slight deviation in the number of small particles detected, which dominate the number density determination, to affect the measurement of the mass flux. The plots in figure 2.23 support this statement. At each axial position there is quite good agreement between the results obtained with either instrument. Agreement is again best in the central regions of the spray where velocities were purely axial. Superimposed onto the graphs a and c are the independent results obtained using an direct sampling probe. Again there is quite good agreement between all three independent measurements.

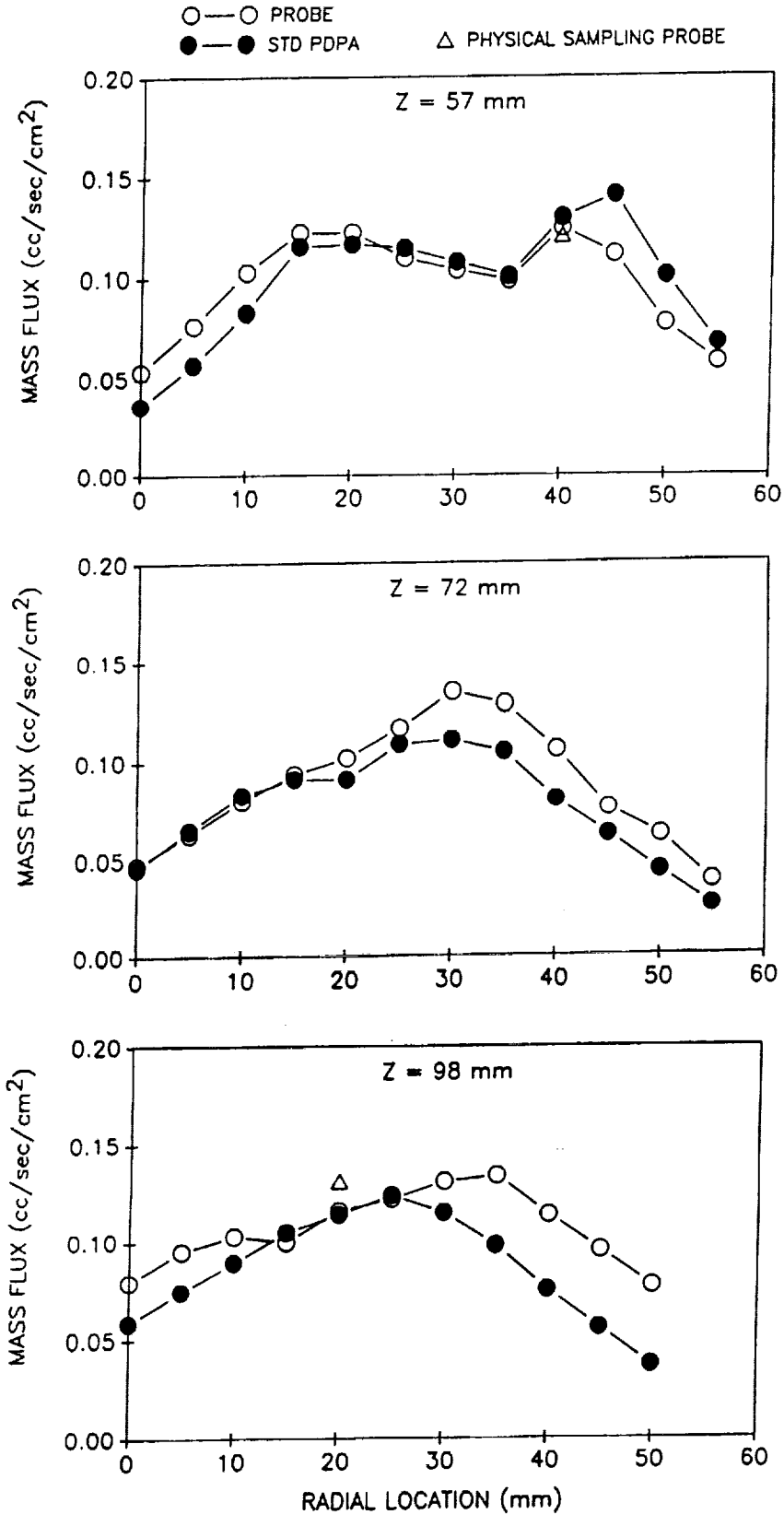

Figure 2.23 Radial Profile of Mass Flux for Fiber Optic Probe, Standard PDPA, and Direct Sampling
a) Z = 57 mm
b) Z = 72 mm
c) Z = 98 mm

2.4.2 The Effect of Crystalline or Irregular Particles on the PDPA Measurement

One of the advantages that the phase Doppler method has over other methods of particle field measurement is that its validation logic makes it possible to discriminate between spherical and irregularly shaped particles. This is done by determining the particle size with two separate sets of detectors as a redundant measurement. The size measured by the two detectors, which have different spacings and sensitivities, are compared. Irregular, non-spherical particles tend to not agree with the theory for spherical particles and are rejected on the basis of this comparison. The two separate phases are measured and if they are outside of certain error windows (epsilon) in terms of percentage or simply in terms of size bins, they are rejected.

In order to test the affect of nonspherical particles on the instrument performance, a comparison was carried out using styrene copolymer beads as the spherical particles and NaCl crystals as the nonspherical particles. Beads were used rather than drops as their concentration and number density could be more easily controlled in this test. It should be noted that beads often contain inclusions or bubbles which invalidate their size measurement and hence, the amount of rejections for beads is higher than for similarly sized water drops.

Measurements were made of each at three different epsilon acceptance criteria. Figure 2.24 displays the

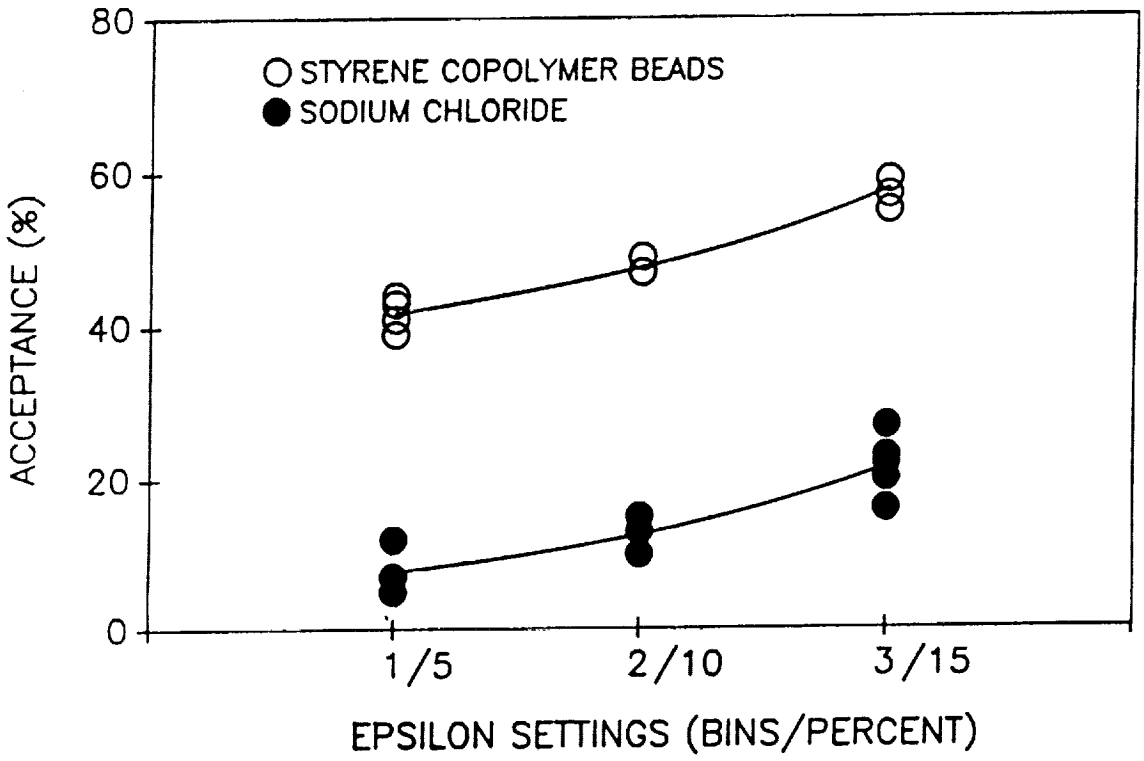

Figure 2.24 Percent Acceptance of NaCl and Styrene Copolymer Beads for Varied Acceptance Criteria

results of these tests. With each decrease in the epsilon settings comes a more stringent requirement that the two independent size measurements obtained by the instrument agree. The plot shows the ratio of the number of valid events to the total number of events detected. The results show as the epsilon settings are decreased, the total change in the number of accepted events for the spherical particles goes down by 27 percent whereas the acceptance ratio for nonspherical particles decreases by 65 percent. Figure 2.25 shows two representative distributions for the spherical beads and the NaCl crystals.

Measurements were also made using an ultrasonic particle generator and simultaneously dispersing NaCl crystals through the measurement volume. A measurement with and without NaCl is shown in figure 2.26. The presence of a bimodal velocity distribution in 2.26b indicates that some crystals were being measured, but the effect on the actual data distribution is negligible. It appears that even though some particles are being measured, their number is very small and thus they do not contribute significantly to the results that would be obtained in the absence of non-spherical particles.

2.5 AEDC Instrument Comparison Test

In May of 1988 a comparison of the standard PDPA instrument to other commonly used cloud droplet size distribution measuring instruments was conducted at Arnold Engineering Development Center (AEDC). In addition to

A)

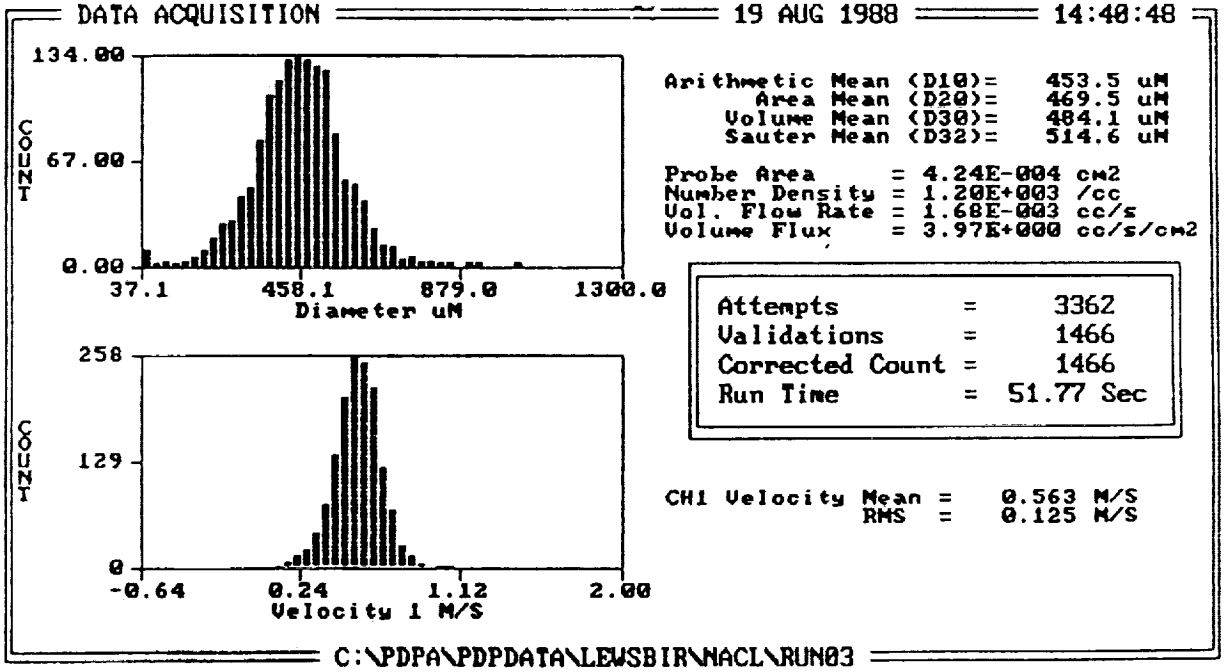

B)

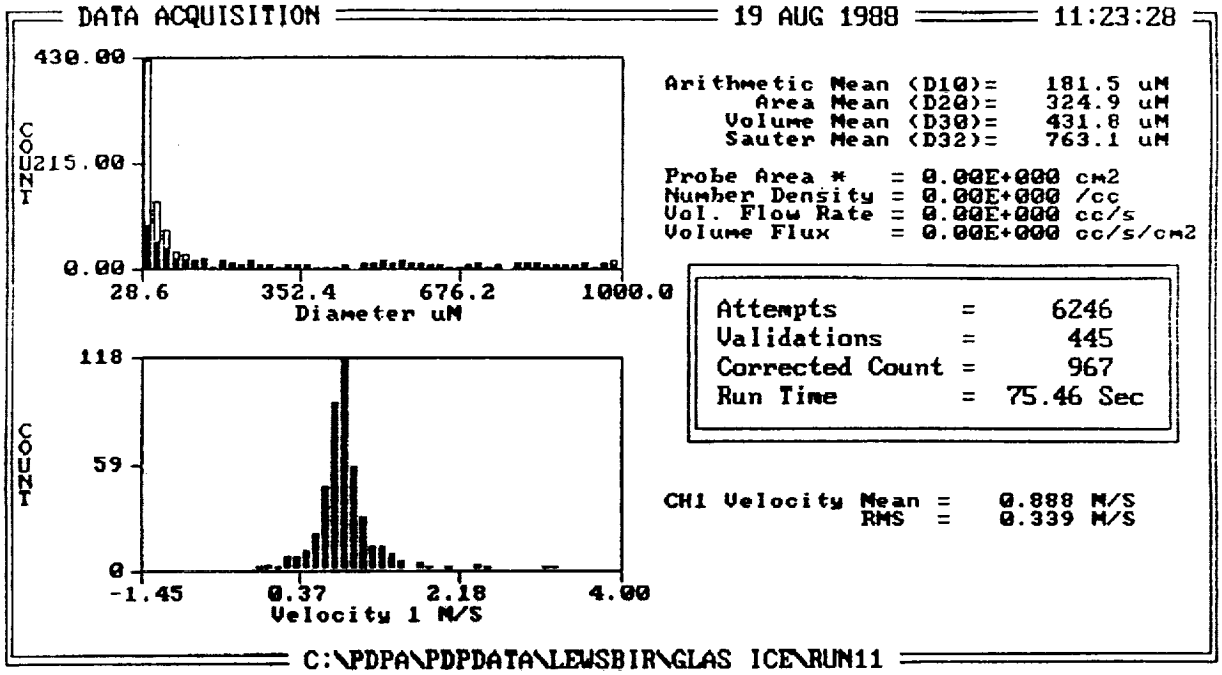

Figure 2.25 Representative Size Distributions
a) Styrene Copolymer Beads
b) NaCl Crystals

A)

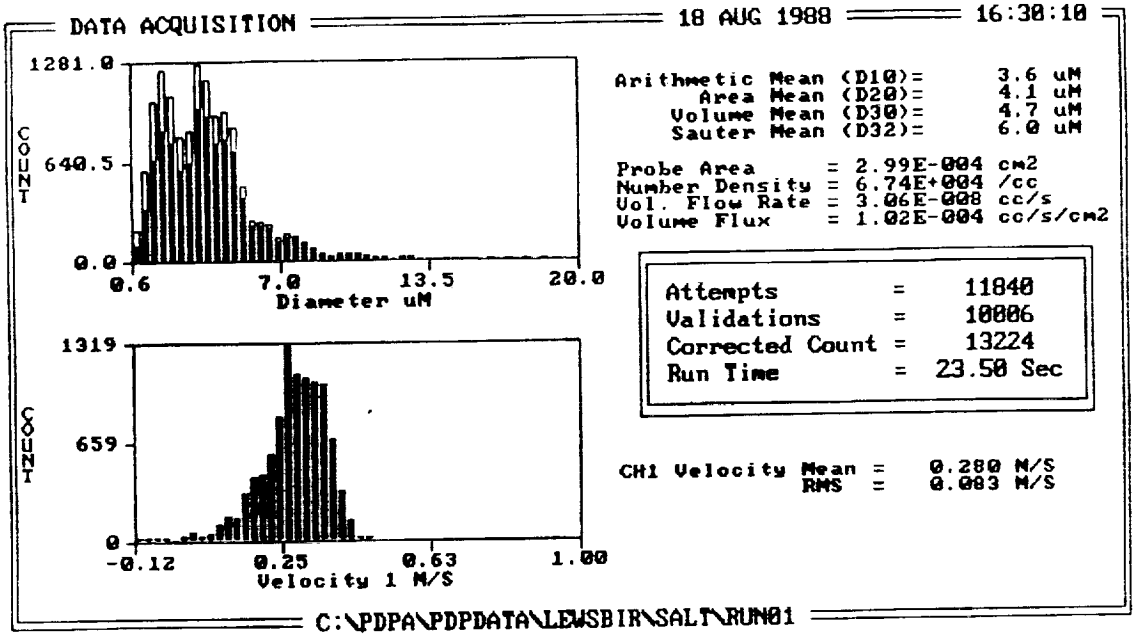

B)

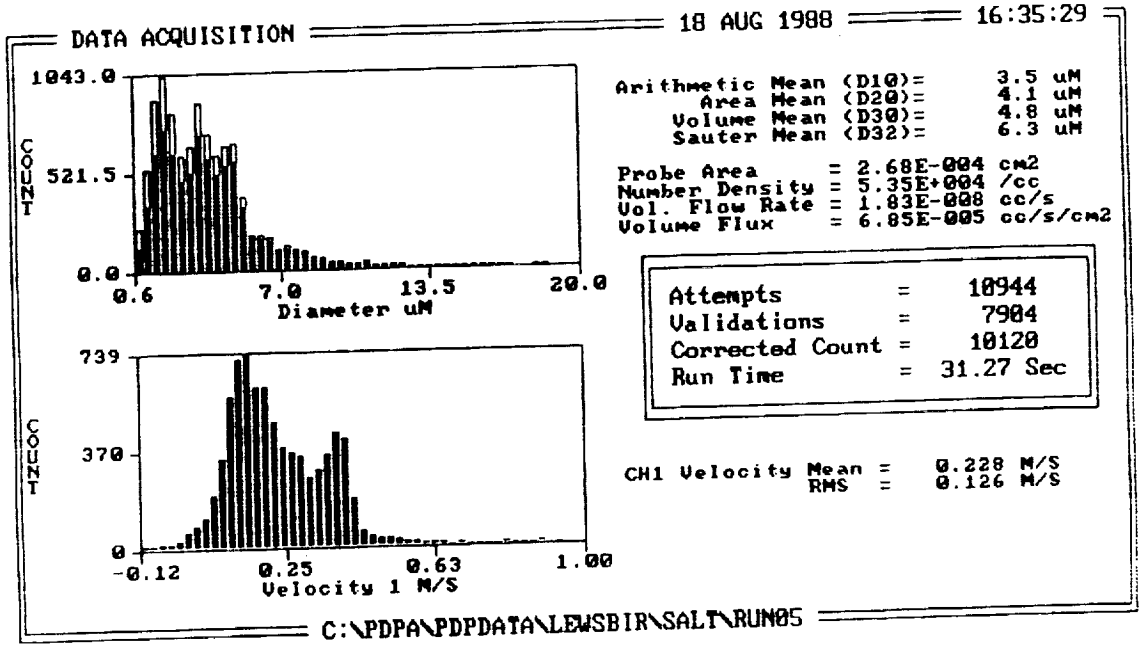

Figure 2.26 Simultaneous Measurement of Water Drops and NaCl
a) No NaCl Present
b) NaCl Present

Aerometrics participation, NASA Lewis, the FAA, the U.S Army, and AEDC were represented at the test. The final result of this comparison is being compiled by Dr. Jim Riley of the FAA Technical Center and should be the subject of a paper at the January, 1989 AIAA Aerospace Sciences Meeting. The test will be described in this report along with some general observations of the testing results and any potential problems.

Background

Since ice accretion on aircraft is quite sensitive to cloud droplet median volumetric diameter (MVD) and size spectrum, monitoring of these quantities is necessary during tests in simulated and actual icing environments. The instruments presently utilized for these measurements have been shown to be inconsistent both from one another and with the present icing certification criterion (FAR Part 25) using a rotating cylinder. Hence, it is necessary to conduct further testing of instruments to establish their sizing characteristics. In addition, this testing allows the inclusion and comparison of the latest phase Doppler method of the PDPA with previously existing measurement instruments.

To meet these requirements the following test objectives were set:

1) A direct comparison of the following particle sizing techniques:
   a) Particle Imaging
   b) Forward Scatter Spectrometry
   c) Phase Doppler Sizing and Velocity
2) Directly compare the instruments sizing capability as a function of velocity, particle size distribution, number density, and the presence of ice particles.
3) Compare the output of extended sizing range instruments to the interpolated and merged output of more limited range instruments.

Facilities

Testing was conducted in the R1D test cell at AEDC. This facility is shown schematically in figure 2.27.[34] The test cell is capable of speeds to Mach 0.7 and pressures from atmospheric to 40 psia. The temperature may be lowered to -20° F. Up to four nozzles may be mounted at the upstream water injection plane and they form a relatively uniform spray (simulated cloud) at the windowed measurement plane of the test cell. Nozzles tested include the NASA Lewis IRT standard, The IRT Mod-1, and a Sonicore 125-H. These are all twin fluid atomizing nozzles.

The PMS type instruments (FSSP and OAP) were sting mounted intrusively in the downstream 3 foot diameter chamber. Windows were provided for the AEDC imaging and PDPA probes at the measurement plane.

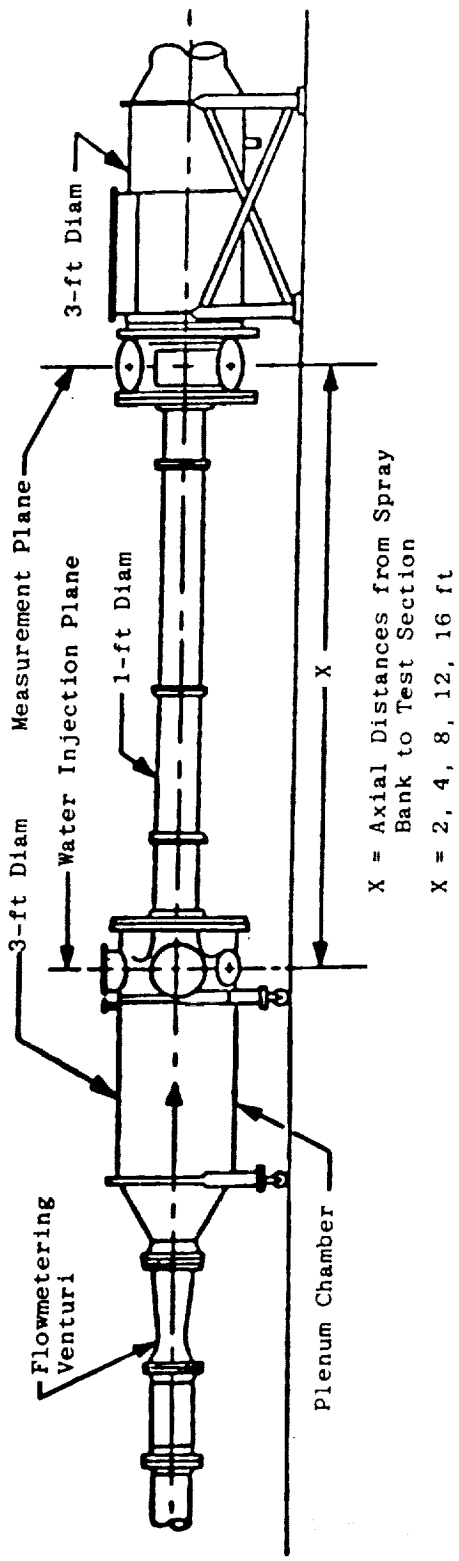

Figure 2.27 AEDC R1D Test Cell[34]

Instrument Features

The comparison was intended to encompass four instruments. As was previously mentioned, these instruments although in use for quite some period of time, suffer from many potential limitations which the PDPA seeks to address. The descriptions of these instruments are compiled from References 12 and 14 which both deal with previous comparison tests.

First was the PMS Forward Scatter Spectrometer Probe (FSSP) and second, the PMS Optical Array Probe (OAP). Both of these probes are intrusive for this application and were mounted in the downstream test chamber. The FSSP was the extended range model and sensitive from roughly 2 to 47 um. The FSSP requires frequent calibration, does not determine a size-velocity correlation and is in fact affected by one, cannot discriminate ice crystals and perturbs the velocity field significantly.[13] It is limited to low number densities and tunnel measurements are already at or beyond its capability. Laser intensity changes due to misalignment, cloud density changes, or wet optics can result in sizing errors. Finally, the LWC measurement is extremely sensitive to optical alignment and the resulting sample area changes.

The OAP imaging probe is theoretically limited to particles ranging from 25 to 300um due to resolution constraints when imaging. However in practice the two smallest size bins of 25 and 45 um are not used as they have

poor resolution (+/- 10 um), and a large sample area correction. Hence there is no practical diameter range overlap with the FSSP. Depth of field effects can also affect the measurements. Again the instrument is limited to low number densities, and in fact, sizing errors will occur for multiple drops in the sample area. A theoretical, rather than experimentally measured, sample area correction must be applied to the data to determine the LWC.

The third instrument was the AEDC Fiber Optic Sizing (FOS) system which is a non-intrusive imaging based system based upon a drop's shadow falling on a fiber optic array. The number of sensors occluded by each drop is directly related to the size of the drop in a manner similar to the OAP. The FOS is operated with a high magnification and has a theoretical size range of approximately 3 to 40 um. However, as would be expected in an imaging system, resolution below 5 um is quite poor due to diffraction limits and electro-optical noise. It also suffers from many of the same liabilities as the commercial OAP in terms of depth of field, high number density performance and a limited size range.

Finally, the standard, full size, PDPA was also installed in the test cell. Note that for optical access in the AEDC test cell a collection angle of 20^{o} was utilized instead of the standard 30^{o}. The phase-size relationship was recalculated for this new angle using an Aerometrics developed scattering code. The accuracy of the phase-size

relationship at 20^{o} was checked via calibration with monodispersed droplets and practical sprays of known size distributions. As was earlier discussed the PDPA offers numerous advantages over existing instruments. Its size range is much larger (100:1 optical, 35:1 dynamic) and is easily varied and overlapped. The sizing is not dependent on intensity and may be performed in high number density environments. The sample area is measured on-line for the actual experiment and the instrument does not require frequent calibration or alignment.

Also due to the test cell size, the instrument used non optimal focal length optics to allow optical access. This had the effect of creating a larger probe volume than would be desirable under ideal conditions. The instrument sensitivity was also somewhat less than ideal for the desired 2.5 - 90 um size range of expected drops that the instrument was configured for. This led to somewhat more rejections due to poor SNR, particularly at high velocities due to the greater than optimal beam waist and correspondingly weaker sample volume intensity. There were an excess of fringes in this overly large probe volume which tended to overflow the counters. The larger probe volume also led to some rejections due purely to multiple particles being in the probe volume. Note that the PDPA will not size and misplace multiple particles in the size distribution. Instead, the PDPA validation logic will reject these multiple occurrences. In an ideal experiment, if time had

been available, the instrument configuration could have been tailored to minimize rejection to a much greater degree.

Test Matrix

The following parametric variations were planned in this study:

1) Particle sizing as a function of air velocity
2) Particle sizing as a function of number density
3) Particle sizing as a function of size distribution
4) Particle sizing in the presence of ice crystals
5) Particle sizing without intrusive probe disturbance
6) Particle sizing as a result of merging data
7) Particle sizing as a function of atomizing air
8) Instrument response to known size glass beads

In the following section some general observations concerning the initial results of this test will be made. The data from the other instruments is still under analysis and only general trends for these instruments will be reported. Note that tunnel velocities were reported by the PDPA that were very close to the values established by AEDC. The smaller particles were seen to be somewhat slower than the bulk velocity and this is due to the perturbation effects of the PMS probe which was located 2 cm behind the PDPA probe volume. Figure 2.28 shows the instrument set-up and a representative size-velocity correlation.

Note that the ability to discriminate individual particle sizes and velocities are important to ensure

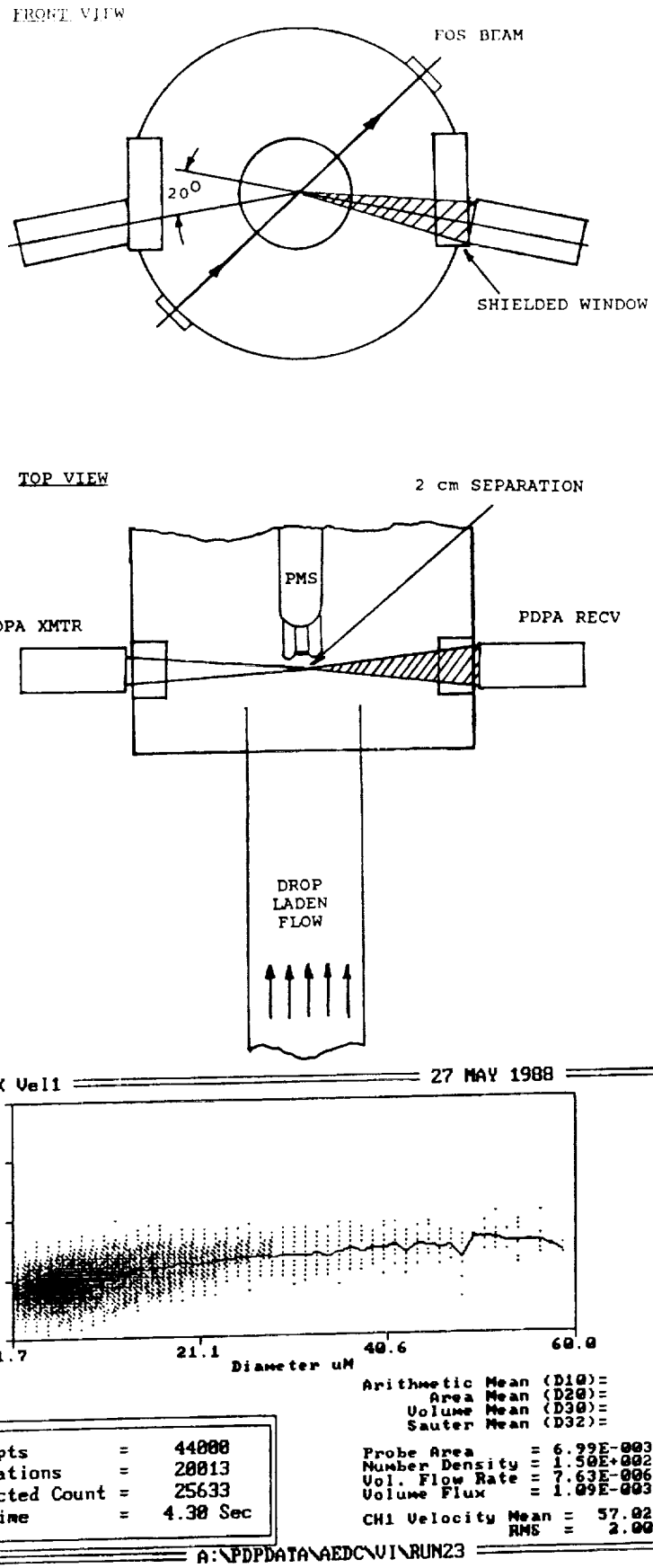

Figure 2.28 AEDC Instrument Set-Up and Representative Size-Velocity Correlation

unbiased measurements. This can especially be a potential problem on aircraft where the influence of the wing or fuselage can alter the velocity and trajectory of the flow. The PDPA will allow fine tuning probe position to eliminate this correlation, or in cases where this is impossible, it may be possible to convert the PDPA data from the temporal measurement, to a spatial measurement that is unbiased by velocity. Details on this are given in reference 4. In either case, an instrument such as the FSSP, in which the accuracy is affected by a size-velocity correlation has no way of knowing if its collecting biased data.

Results

Examining response of the PDPA to bulk air flow velocity (Test 1), figure 2.29 shows that both the Arithmetic Mean Diameter, D_{10}, and the MVD were quite flat in response over the entire operating range of 30 to 95 m/s for two different nozzle spray conditions. The size-velocity correlation, as was shown in figure 2.28, strengthened at higher velocities and this should have a deleterious affect on the FSSP performance as velocity increases.

Looking at the effect of number density (Test 2), from 1-4 nozzles can be run in the test cell. Again, as is shown in figure 2.30, PDPA size response to increasing number density was quite flat. It should be noted that the nozzles were spread fairly far apart and the size distributions were

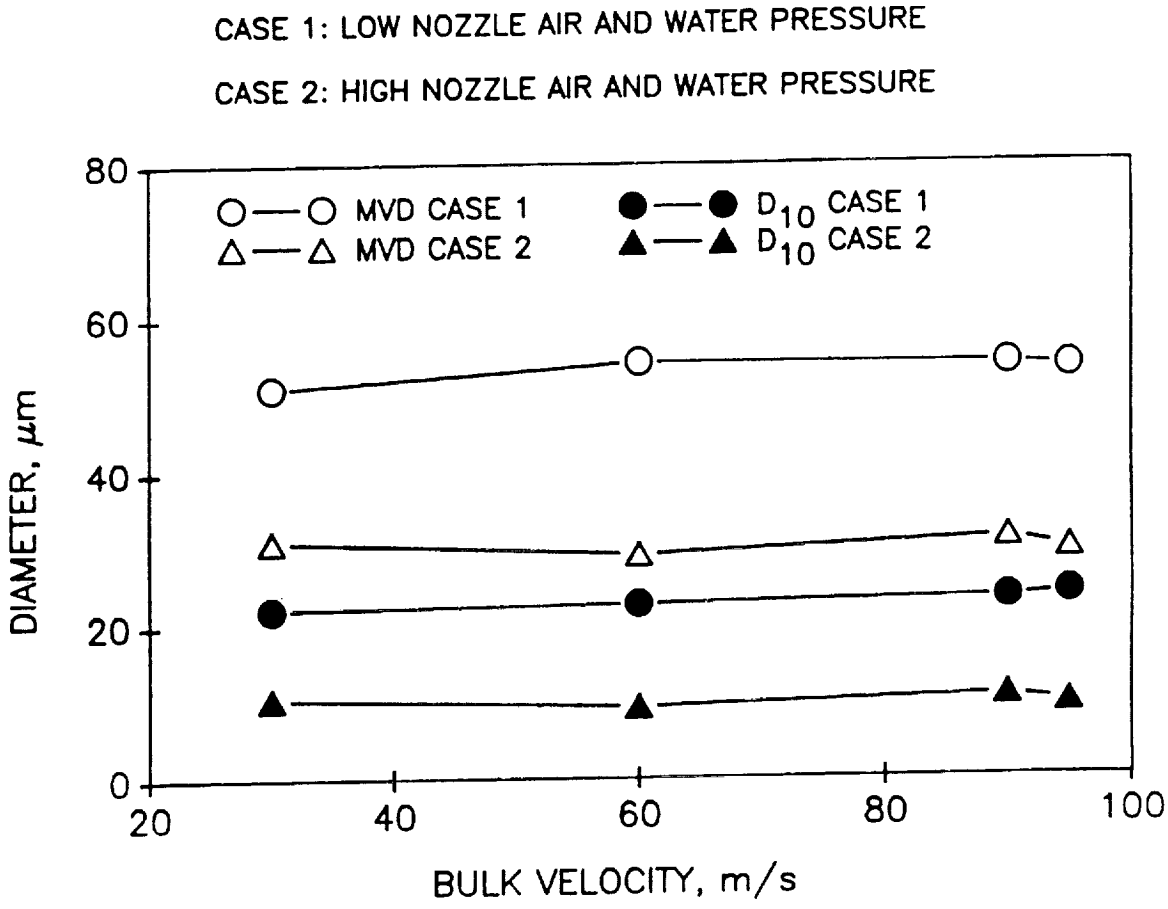

Figure 2.29 D_{10} and MVD versus Bulk Air Velocity

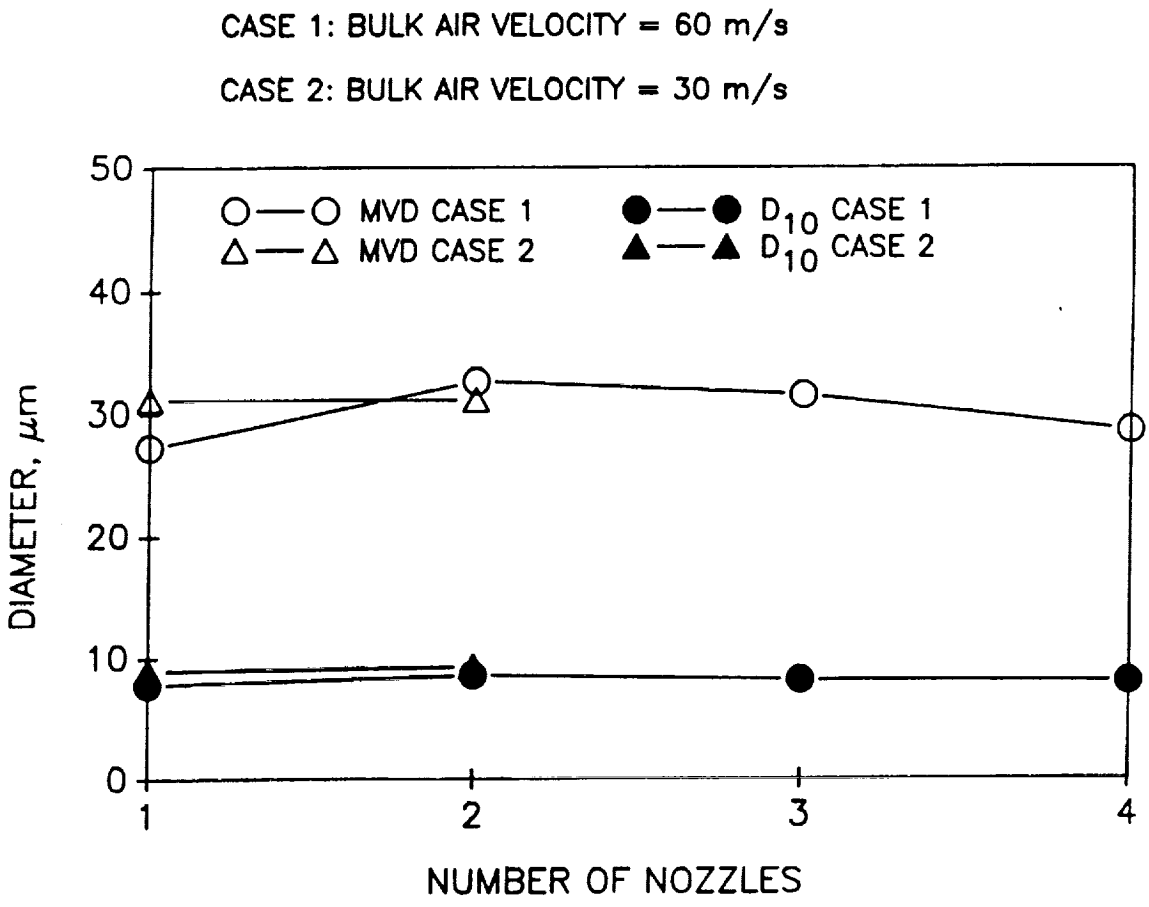

Figure 2.30 D_{10} and MVD versus Droplet Number Density

not necessarily perfectly uniform. Also, it was again seen that bulk air velocity had no effect on the PDPA results.

Test 3 and Test 7 both looked at the response of the instruments to differing size distribution. Shown in figure 2.31 is a plot of D_{10} and MVD versus atomizing air pressure for a constant nozzle water flow rate. As would be expected for a twin fluid nozzle, higher air pressures atomized well, while the lower pressures had a long tail of larger, poorly atomized drops. Figure 2.32 shows sample of this behavior in terms of both number and volume. Note the very strong contribution to volume (and MVD!) due to a very small number of larger drops. The FSSP and the FOS both showed no evidence of this tail, but its existence at low nozzle air to fuel ratios is well documented among spray researchers.[27] As will be discussed shortly, both these instruments did not respond well to these larger drops.

No apparent problems were seen in the tests at temperatures below freezing where ice crystals might have occurred (Test 4). Test 5 was eliminated as icing of the PMS probe occluded its view ports and even built up enough on the probe too block the PDPA beams 2 cm in front of the probe. Although no data was stored, observations of the size-velocity correlation with the PMS probe removed showed a flat or uncorrelated size-velocity correlation.

In test 6, the study of merging the PMS probe distributions, Aerometrics is still waiting for the FAA report on the test.

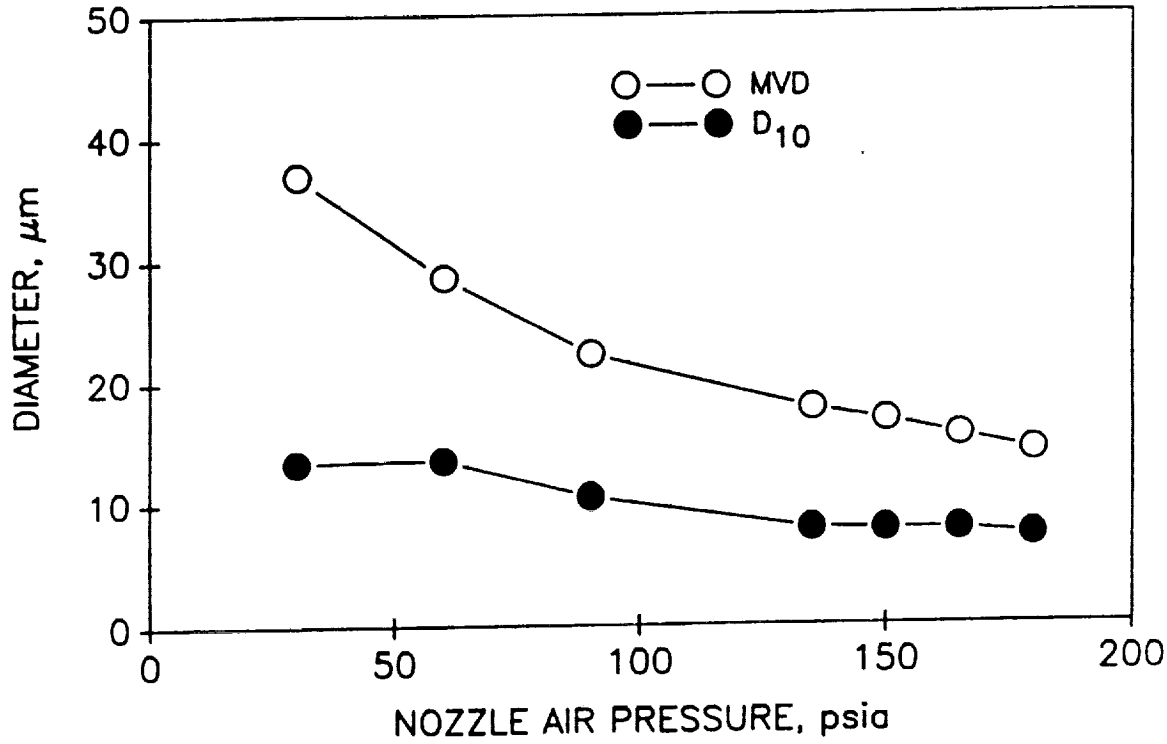

Figure 2.31 D_{10} and MVD versus Atomizing Air Pressure

A)

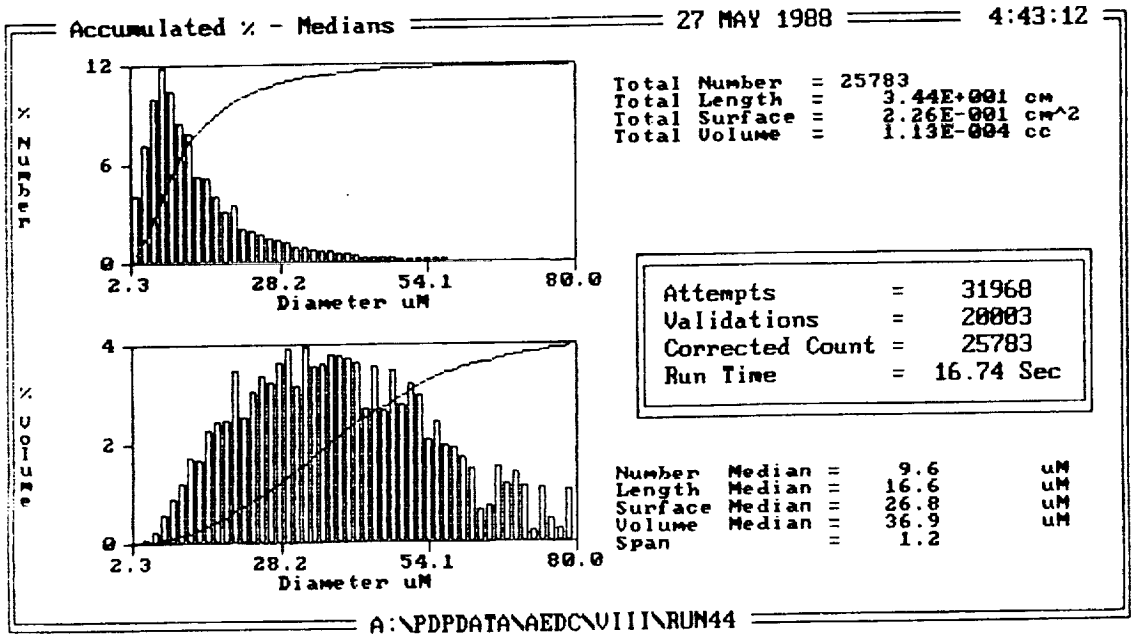

B)

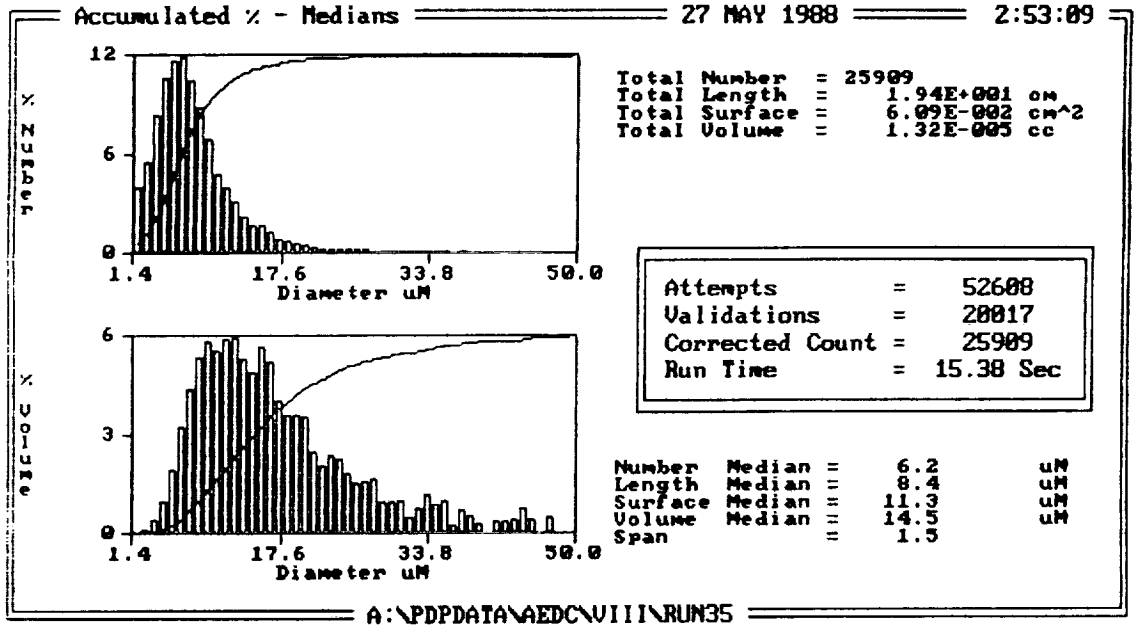

Figure 2.32 Cumulative Distributions of Number and Volume
a) Low Nozzle Air Pressure
b) High Nozzle Air Pressure

Finally, to illustrate the accurate response of the PDPA, glass beads of known size ranges were passed through the sample volume of each probe. The PDPA response illustrated in figure 2.33 shows quite accurate sizing for beads in the ranges of 15-37 um, 44-53 um, and nominal 100 um. In comparison the FSSP and FOS, while agreeing reasonably with the PDPA for the smallest size class, also placed the larger beads in quite small and clearly incorrect size classes. This reinforces the earlier discussed PDPA measurement of extended tails of large size drops for many of the size distributions that were not detected by the other two probes. Hence, the PDPA determined MVD was larger than the other two instruments under many conditions.

In addition, rough calculations of LWC for the R1D test cell were made by Mr. Scott Bartlett of Sverdrup at AEDC. The PDPA calculations showed good qualitative agreement with his calculations, but they are necessarily qualitative as the spray distribution was not truly uniform in the tunnel.

In terms of problems noted while conducting the test, they were mainly related to the probe volume size not being ideal for the testing condition. If sufficient time had been available to optimize the PDPA setup, this difficulty could have been easily mitigated. Overall, it was seen that the standard PDPA showed excellent behavior and response in measuring simulated cloud environments. In larger tunnels, such as the Lewis IRT or in practical airborne environments

A)

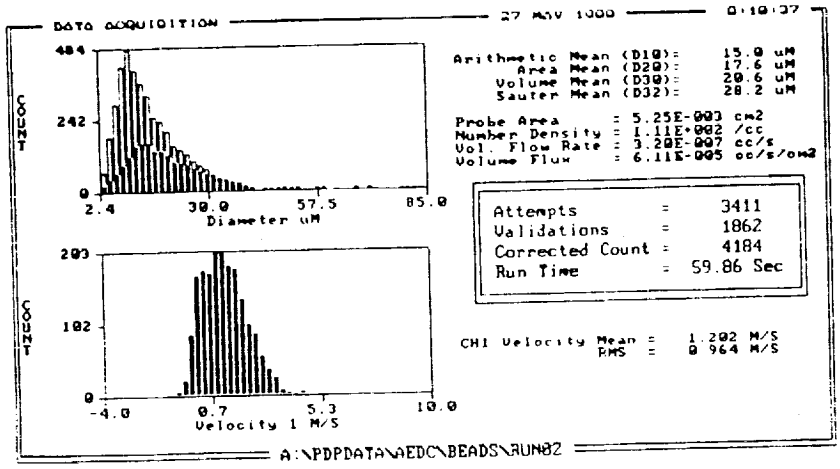

B)

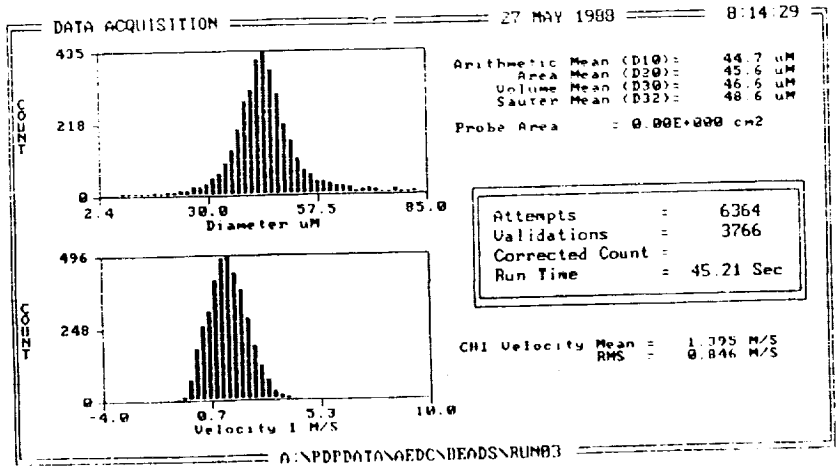

C)

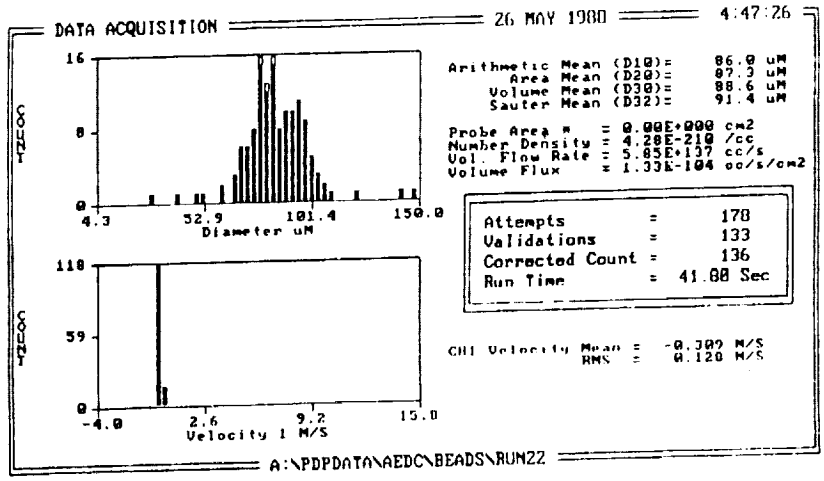

Figure 2.33 PDPA Measurements of Glass Beads
a) 15-37 um
b) 44-53 um
c) Nominal 100 um

a more compact probe that may be mounted in the flow is necessary to optimize the optical setup. Testing of the compact fiber optic probe prototype was conducted at the Lewis IRT and is discussed in the following section.

2.6 IRT Instrument Feasibility Test

In July 1988 the opportunity arose to 'piggyback' a feasibility test of the prototype PDPA fiber optic probe with other testing being performed by NASA and the Army in the Icing Research Tunnel (IRT) at NASA Lewis. The prototype probe was mounted in the IRT 6' x 9' test section along with NASA and Army OAP and FSSP probes. The objective of this test was primarily to establish the feasibility of utilizing the fiber optic PDPA probe in a simulated cloud environment. Potential problems were to be discovered and the probe performance characterized. The final objective was to determine potential solutions to the problems that were certain to occur in the first in situ test of the probe.

The prototype probe as described in section 2.2, although water proof and fairly rugged, was not designed to be mounted in high speed and cold air flows. Nevertheless, a mount was designed and the probe mounted in the IRT, figure 2.34. Hoods with nitrogen purge kept the windows moisture free.

Testing was largely performed at 120 knots (61.7 m/s), a speed comparable to the previous AEDC test baseline speed. Some testing was also done at lower velocities. The total

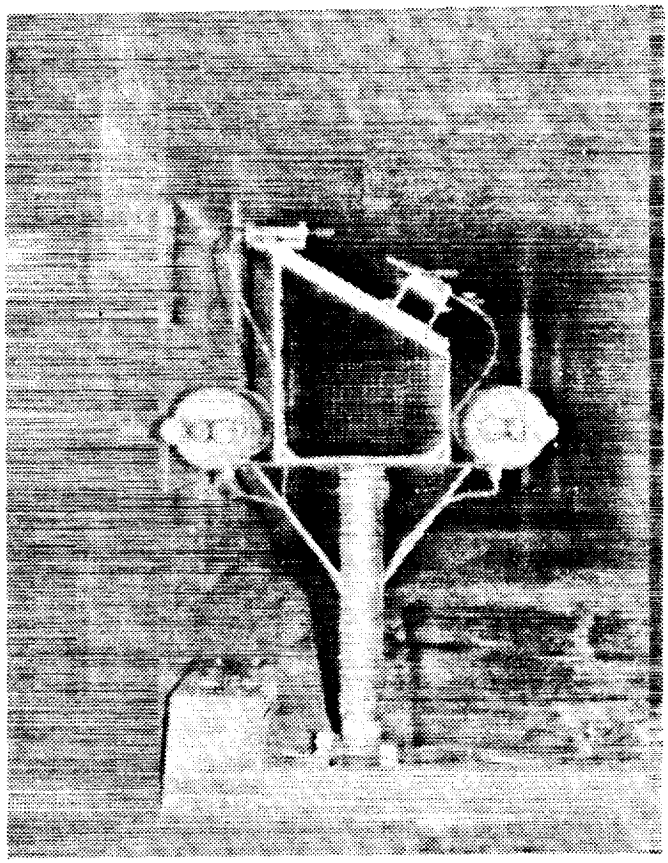

Figure 2.34 Fiber Optic Probe Mounted In the IRT

tunnel temperature was 20° F. The probe was found to have icing in the regions over the hoods, but in general the actual aperture stayed clear. No moisture was found at any time on the interior of the probe, though unnoticed condensation must be considered a possibility.

Aside from expected design inadequacies, results of the testing were surprisingly satisfactory. At no time during several days of testing did ice accretion prevent data acquisition. The cold temperatures experienced by the probe during this test did not affect performance of the optics or the optical fibers. When properly aligned, drop signals observed on a digital storage scope were of high signal-to-noise ratio, even though less than 1mw of laser power was available in each incident beam.

Data obtained during the test showed no loss of sensitivity to small drops at high velocities, figure 2.35. The results, in general, compared favorably with those obtained with the FSSP probes, although the (2) FSSP probes did not always agree between themselves. FSSP data was reported only as a a Median Volumetric Diameter (MVD) and the size sensitive range of the FSSP probes was limited to a maximum of 47 um. MVD is weighted by the cube of the particle diameter and is easily perturbed by the addition or deletion of larger sized drops. The PDPA, when opened to 100 um maximum drop size reported drops larger than 47 um, which would be unobservable to the FSSP, yet drastically affect the true MVD.

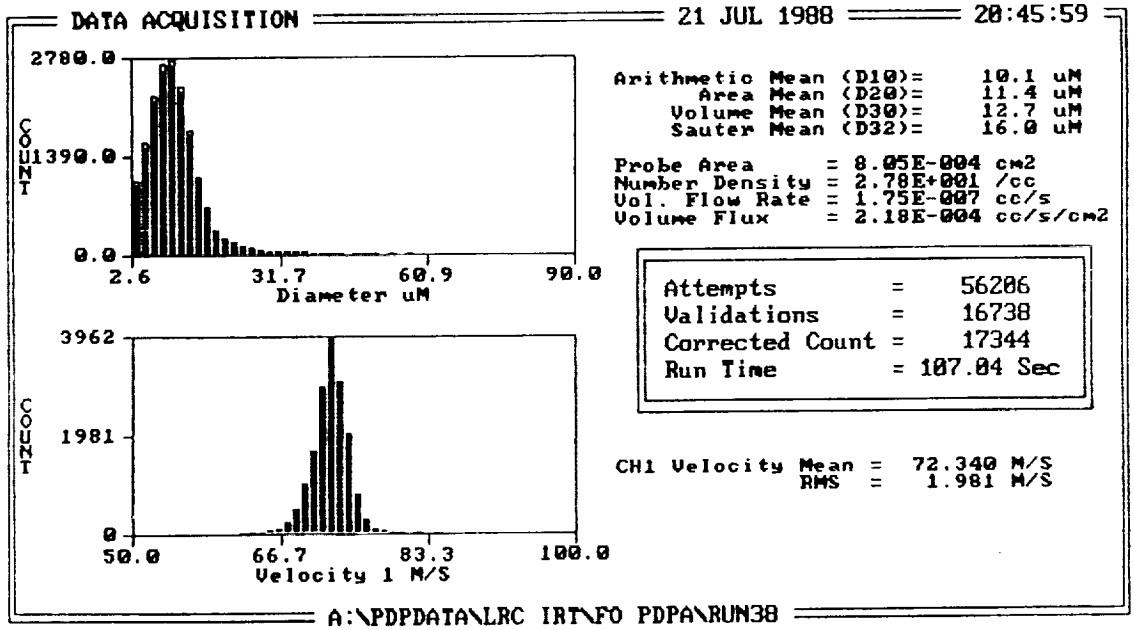

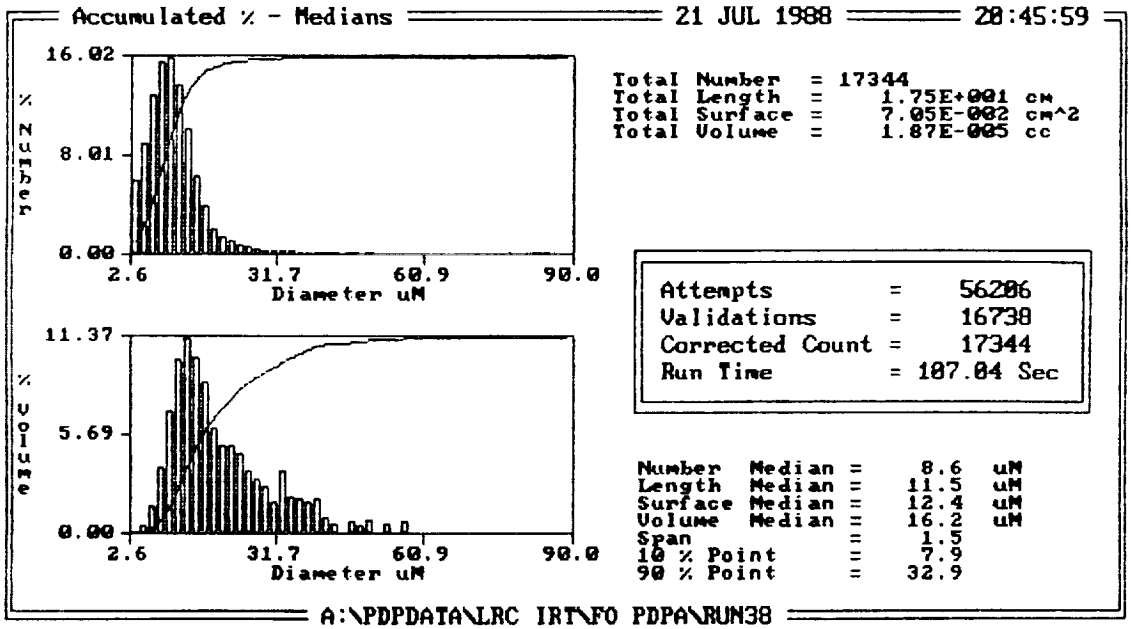

Figure 2.35 Response of Fiber Optic Probe to Small, High Speed Drops

Liquid Water Content (LWC) was also reported by the FSSP probes and calculated from the PDPA measurements. The PDPA consistently underreported the LWC measured by the FSSP. Of concern from a comparative viewpoint during this test was the non-uniformity of particle loading within the tunnel test section. The IRT has several parallel rows of spray bars, each with multiple nozzles, used to introduce drops to the flow. These spray bars have been carefully adjusted to produce a uniform drop cloud of particles when all bars and nozzles are operated. To generate Liquid Water Contents (LWC) within the range of the FSSP probes, alternate spray bars were not used for this test. It was visibly evident during testing that 'bands' of drop-laden clouds were present. The striated bands were separated by low drop density regions. Since the FSSP and PDPA probes were located at different vertical locations, this drop field non-uniformity must necessarily invalidate LWC comparisons.

The PDPA-measured velocities of the drops were consistently higher than the expected tunnel speed and was attributed to test section blockage by the FSSP / PDPA mounting stand (see figure 2.34). Size-Velocity correlations were flat indicating, as expected, uniform drop velocity for all size classes, figure 2.36.

The primary problems were seen in the following areas and will be addressed in the phase II portion of this study in order to build a probe suitable for cold, high speed use

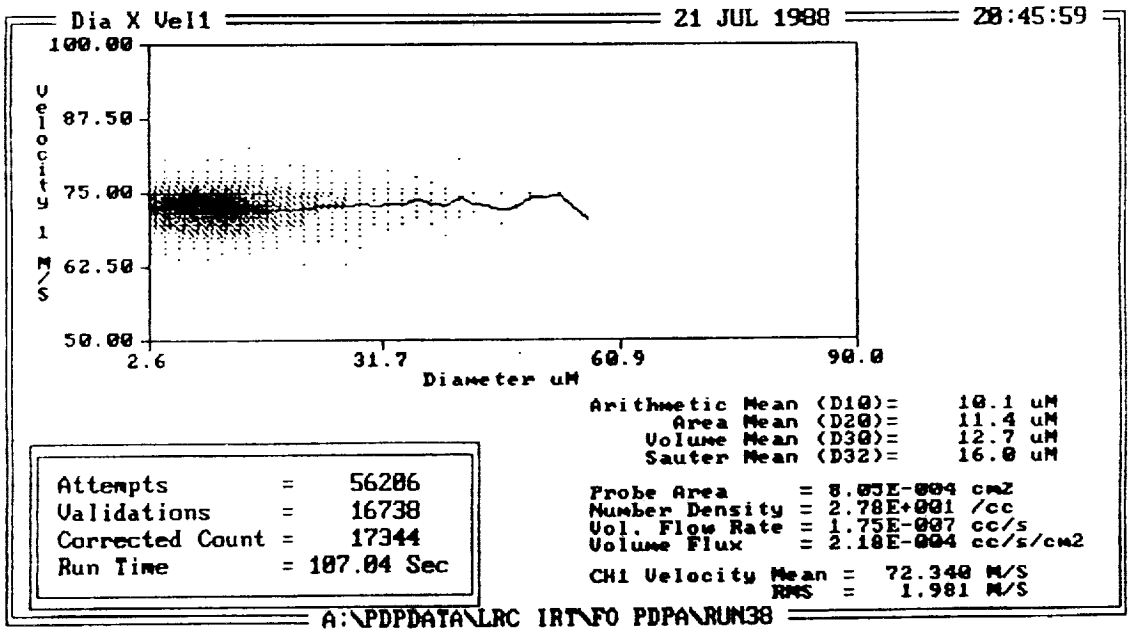

Figure 2.36 Size-Velocity Correlation in the IRT

in both simulated and practical, airborne environments. First, ice formation on the probe was a problem. This was mainly from a convenience and alignment standpoint. The purge air kept the viewing aperture clear, but to make an adjustment, deicing was necessary. The three methods used in the IRT: 1) hitting the probe with a large delrin rod was quick and effective, but too brutal on optical components and their relative alignment, 2) using a steam hose which caused condensation on the windows and possibly internally, or 3) using a heat gun which was too slow. This problem may be addressed by improving the probe design, as detailed in section 4, to include electric deicing.

Next, the external alignment of the receiver must be more rugged to ensure continued alignment. Vibration and high flow velocities work together to change alignment which must be accurate on the order of 10 um. Again, improving the probe design, detailed in the following section, will address this difficulty.

Vibration also affected the internal alignment of the transmitter and would cause phase variation in the two polarization preserving fibers. Both these factors had a deleterious effect on the probe volume quality and fringe contrast resulting in poor signal to noise ratio signals. Thermal effects due to different probe materials having different thermal coefficients of expansion could also affect alignment stability.

These problems will be dealt with by building a probe using only a single fiber to bring the coherent beam to the transmitter. In this way vibration will not effect the phase of the two beams. Beam splitting and focusing will be accomplished by self-aligning prismatic optics located in the transmitter head. Some problems were seen with lens retainers loosening due to vibration and/or temperature which can be solved via better design practice that considers thermal effects. Again section 4 will fully describe this revised probe. Note that no frequency shift will be provided with such a probe, but in wind tunnel or airborne applications, the uniform velocity field precludes the need for any frequency shift.

In addition, the test pointed out that the power presently exiting the transmitter is limited to between 1 and 2 mW per beam. In high speed flows, especially if they reach speeds of up to 300 m/s with small (2- 10 um) drops, additional laser power will be necessary. A number of means exist to produce this higher power including gas lasers or laser diodes. Further study will demand identifying the best means of providing this laser power with the weight limitations of airborne applications kept in mind.

Overall, when it is considered that the prototype probe was not intended to be mounted inside the test section of a icing tunnel at 20 ^{o} F, the PDPA performed quite well. When properly aligned, it was able to make accurate measurements of MVD and size spectra. Most importantly, the test pointed

out the specific elements of the probe which need rework to optimize performance for icing studies in high speed, cold environments.

3.0 SUMMARY AND CONCLUSIONS

A basic, compact, fiber optic-based probe was developed for the Aerometrics Phase Doppler Particle Analyzer for possible applications to aircraft icing research. The probe incorporated all of the features of the standard PDPA including frequency shifting. Thorough testing of the probe, which included direct comparisons of the measured size distributions, number densities, and LWC with the results obtained with the standard PDPA, showed excellent performance.

Although the results of the testing of the basic prototype PDPA fiber optic probe were relatively successful overall, there were areas identified that clearly needed improvement before the probe would be suitable for aircraft icing research applications. These areas, discussed at the close of each section, were largely involved with the transmitter portion of the probe, and came about largely due to the nature of this "proof of concept" study, which entailed the development of a general purpose probe. However, in more specific applications such as icing research where no frequency shift is needed in the transmitter beams, many of the problems can easily be eliminated. Nevertheless, it may be quite beneficial to review some of these difficulties and the various solutions that are available.

The first difficulty encountered was in the polarization of the two beams as they exit the pair of

single mode, polarization-preserving fibers. As mentioned in section 2.2, the ability of the fiber to maintain the polarization of the fiber may be altered by faults in the fiber or by a slight amount of misalignment of the polarization axis of the fiber. As a result, the polarization of a beam that passes through the fiber may have some of its energy in both polarization states. This effect is aggravated by external forces applied to the fiber. As a consequence, if the probe is subject to a high vibration environment the fringes may modulate at a frequency that could affect the probe's ability to perform properly.

Although the actual effect of vibration must certainly be tested, the problem is easily solved for a system that does not require frequency shift, such as one used in icing research. This is true because all of the laser energy can be brought to the probe head by a single fiber and then separated within the probe. This eliminates any fringe movement, which is itself due to unequal response of two individual fibers. Another solution which makes use of a single fiber is to place a Bragg cell within the transmitter (which has the disadvantage of increased size and complexity).

Another problem encountered with this prototype design was a difficulty in keeping the beams exactly crossing at the measurement volume. Due to the nature of the beams, which originate from two optical fibers inside the probe

C-2

head, it was difficult to steer the beams straight so that they intersected perfectly and were parallel. Again this problem disappears when a single source of the laser light is brought directly to the transmitter probe. In such an instance a simple prism beamsplitter can be used to split the beam into two equal intensity parts. If the proper prism is selected, the beams will be perfectly aligned and parallel.

While the current design utilized the standard Aerometrics counter-processor, the high speed and small particles of icing studies, with their associated low signal-to-noise ratio, lend themselves to processing in the frequency domain. This would best be done with the FFT processor under development at Aerometrics. An FFT type processor can handle higher frequencies and poor SNR conditions more reliably and might even mitigate the need for more laser power than the current 10 mW He-Ne.

Finally, improved means of deicing the probe and protecting its optics are necessary. Inclusion of electric deicing on the next probe should eliminate many of the problems seen in the IRT test.

REFERENCES

1. Olsen, W., Shaw, R., and Newton, J., "Ice Shapes and the Resulting Drag Increase for a NACA 0012 Airfoil", NASA Technical Memorandum 83556, January, 1984.

2. Blaha, B. J., and Shaw, R. J., "The NASA Altitude Wind Tunnel: Its Role in Advanced Icing Research and Development", AIAA-85-0090, 1985.

3. Scott, J. N., Hankey, W. L., Giessler, F. J. and Gielda, T. P., "Navier-Stokes Solution of the Flowfield Over Ice Accretion Shapes", AIAA-87-0099, 1987.

4. Potapczuk, M., "Numerical Analysis of NACA0012 Airfoil With Leading Edge Ice Accretions", AIAA-87-0101, 1987.

5. Belte, D., and Ferrell, K. F., "Helicopter Icing Spray System", Preprint 80-52, presented at 36th Annual Forum of the American Helicopter Society, Washington, D.C., 1980.

6. Gent, R. W., and Cansdale, J. T., "The Development of Mathematical Modelling Techniques for Helicopter Rotor Icing", AIAA-85-0336, 1985.

7. Shaw, R. J., and Richter, G. P., "The UH-1H Helicopter Icing Flight Test Program: An Overview", AIAA-85-0338, 1985.

8. Belte, D., and Woratschek, R., "Helicopter Icing Spray System (HISS) Evaluation and Improvements", USAAEFA Project No. 82-05-3 Final Report, April, 1986.

9. Belte, D., "In-Flight Ice Accretion Characteristics of Rotor Blade Airfoil Test Sections", AIAA-87-0176, 1987.

10. Turner, F. M., and Radke, L. F., "The Design and Evaluation of an Airborne Optical Ice Particle Counter", J. of Applied Meteorology, Vol. 12, No. 8, pp. 1309-1318, December, 1973.

11. Knollenberg, R. G., "Techniques for Probing Cloud Microstructure", Clouds: Their Formation, Optical Properties, and Effects, pp. 15-91, Academic Press, 1981.

12. Hunt, J. D., "A Comparison of Particle Diagnostic Systems", AEDC-TR-80-33, August 1981.

13. Hovenac, E. A., "Operating Envelopes of Particle Sizing Instrumentation Used for Icing Research", AIAA-88-0291, January, 1988

14. Takeuchi, D. M., Jahnsen, L. J., Callandar, S. M., and Humbert, M. C., "Comparison of Modern Icing Cloud Instruments", NASA Contractor Report 169008, January, 1983.

15. Bachalo, W. D. and Houser, M. J., "Development of the Phase-Doppler Spray Analyzer for Liquid Drop Size and Velocity Characterization", AIAA 84-1199, 1984.

16. Bachalo, W. D., Houser, M. J., and Smith, J. N., "Behavior of Sprays Produced by Pressure Atomizers as Measured Using the Phase Doppler Instrument", Atomization and Spray Technology, Vol. 3, pp.53-72, 1987.

17. Bachalo, W. D., "Methods for Measuring the Size and Velocity of Spheres by Dual-Beam Light Scatter Interferometry", Applied Optics, Vol. 19, No. 3, 1980.

18. van de Hulst, H. C., Light Scattering by Small Particles, Wiley, New York, 1957.

19. Young, B. W. and Bachalo, W. D., "The Direct Comparison on the 'In-Flight' Droplet Sizing Techniques for Pesticide Research", presented at The International Symposium on Optical Particle Sizing, Rouen, France, 1987.

20. Jackson, T. A. and Samuelsen G. S., "Droplet Sizing Interferometry: A Comparison of the Visibility and Phase Doppler Techniques", Applied Optics, Vol. 26, No. 11, pp. 2137-2143, 1987.

21. Mcdonell, V. G., Wood, C. P., and Samuelsen, G. S., "A Comparison of Spatially Resolved Drop Size and Drop Velocity Measurements in an Iso-Thermal Chamber and Swirl-Stabilized Combustor", presented at 21st Symposium (International) on Combustion, Munich, West Germany, August, 1986.

22. Dodge, L. G., "Comparison of Performance of Drop Sizing Instruments", Applied Optics, Vol. 26, No. 7, April, 1987.

23. Dodge, L. G., " The Physics of Fuel Sprays, Vol. 1 - Experimental Measurements", SwRI Interim Report 885811, 1986.

24. Bachalo, W. D. "Diagnostics Development for the Characterization of Liquid Fuel Rocket Engine Injector Atomization", NASA Phase I Contractors Report, 1987.

25. Bachalo, W. D., Brena de la Rosa, A., and Rudoff, R. C., "Diagnostic Development For Spray Characterization in Complex Turbulent Flows",, ASME 88-GT-241, presented at 33rd International Gas Turbine Conference, Amsterdam, Netherlands 1988.

26. Bachalo, W. D., Rudoff, R. C., and Brena de la Rosa, A., " Mass Flux Measurements of a High Number Density Spray System Using the Phase Doppler Particle Analyzer", AIAA 88-0236, 1988.

27. Lefebvre, A. H. Gas Turbine Combustion, Hemisphere Publishing, 1983.

28. Noda, J., Okamoto, K., and Sasaki, Y., "Polarization Maintaining Fibers and Their Applications", Journal of Lightwave Technology, Vol. 4, No. 8, pp. 1071-1089, 1986.

29. Dyott, R. B., Cozens, J. R., and Morris, D. G., "Preservation of Polarization in Optical-Fiber Waveguides with Elliptical Cores", Electronic Letters, Vol. 17, No. 13, pp. 473-474, 1981.

30. Okamoto, K., Hosaka, T., and Noda, J., "High Bi-Refringence Polarizing Fiber with Flat Cladding", J. Lightwave Technology, Vol. LT-3, No. 4, pp. 758-762, 1985.

31. Birch, R. D., Varnham, M. P., Payne, D. N., and Tarbox, E. J., "Fabrication of Polarization-Maintaining Fibers Used for Laser Diode Redundancy in a Submarine Optical Repeater", Electronic Letters, Vol. 18, No. 24, pp. 1036-1038, 1982.

32. Fiber Property Specification Sheet, Fujikara Ltd., June, 1986.

33. Fiber Property Specification Sheet, York V.S.O.P. Inc., July, 1986.

34. AEDC Technical Resources and Services, No. 86-1, April, 1986.

NASA
National Aeronautics and Space Administration

Report Documentation Page

1. Report No.	2. Government Accession No.	3. Recipient's Catalog No.
NASA CR-185225		

4. Title and Subtitle	5. Report Date
Advanced Instrumentation for Aircraft Icing Research	April 1990
	6. Performing Organization Code

7. Author(s)	8. Performing Organization Report No.
W. Bachalo, J. Smith, and R. Rudoff	None
	10. Work Unit No. 505-68-11

9. Performing Organization Name and Address	11. Contract or Grant No.
Aerometrics, Inc. 894 Ross Drive, Unit 105 Sunnyvale, California 94089	NAS3-25317
	13. Type of Report and Period Covered Contractor Report Final

12. Sponsoring Agency Name and Address	14. Sponsoring Agency Code
National Aeronautics and Space Administration Lewis Research Center Cleveland, Ohio 44135-3191	

15. Supplementary Notes

Project Manager, John R. Oldenburg, Propulsion Systems Division, NASA Lewis Research Center.

16. Abstract

A compact and rugged probe based on the phase Doppler method was evaluated as a means for characterizing icing clouds using airborne platforms and for advancing aircraft icing research in large scale wind tunnels. The Phase Doppler Particle Analyzer (PDPA) upon which the new probe was based is now widely recognized as an accurate method for the complete characterization of sprays. The prototype fiber optic-based probe was evaluated in simulated aircraft icing clouds and found to have the qualities essential to providing information that will advance aircraft icing research. Measurement comparisons of the size and velocity distributions made with the standard PDPA and the fiber optic probe were in excellent agreement as were the measurements of number density and liquid water content. Preliminary testing in the NASA Lewis Icing Research Tunnel (IRT) produced reasonable results but revealed some problems with vibration and signal quality at high speeds. The cause of these problems were identified and design changes were proposed to eliminate the shortcomings of the probe.

17. Key Words (Suggested by Author(s))	18. Distribution Statement
Fiber optics; Droplet sizing; Particle sizing; Aircraft icing; Phase Doppler; Liquid water content	Unclassified – Unlimited Subject Category 06

19. Security Classif. (of this report)	20. Security Classif. (of this page)	21. No. of pages	22. Price*
Unclassified	Unclassified	101	A06

*For sale by the National Technical Information Service, Springfield, Virginia 22161